



REFERENCE ONLY

# Calculations of Turbulent Boundary Layer (TBL) Pressure Fluctuations Transmitted into a Viscoelastic Layer

Sung H. Ko  
Howard H. Schloemer  
Submarine Sonar Department

REFERENCE ONLY



**Naval Underwater Systems Center**  
Newport, Rhode Island/New London, Connecticut

Approved for Public Release; distribution unlimited.

REFERENCE ONLY

Report Documentation Page			Form Approved OMB No. 0704-0188		
Public reporting burden for the collection of information is estimated to average 1 hour per response, including the time for reviewing instructions, searching existing data sources, gathering and maintaining the data needed, and completing and reviewing the collection of information. Send comments regarding this burden estimate or any other aspect of this collection of information, including suggestions for reducing this burden, to Washington Headquarters Services, Directorate for Information Operations and Reports, 1215 Jefferson Davis Highway, Suite 1204, Arlington VA 22202-4302. Respondents should be aware that notwithstanding any other provision of law, no person shall be subject to a penalty for failing to comply with a collection of information if it does not display a currently valid OMB control number.					
1. REPORT DATE <b>21 JUN 1985</b>		2. REPORT TYPE <b>Technical Memo</b>		3. DATES COVERED <b>21-06-1985 to 21-06-1985</b>	
4. TITLE AND SUBTITLE <b>Calculations of Turbulent Boundary Layer (TBL) Pressure Fluctuations Transmitted into a Viscoelastic Layer</b>			5a. CONTRACT NUMBER		
			5b. GRANT NUMBER		
			5c. PROGRAM ELEMENT NUMBER <b>62702E</b>		
6. AUTHOR(S) <b>Sung Ko; Howard Schloemer</b>			5d. PROJECT NUMBER <b>070011</b>		
			5e. TASK NUMBER		
			5f. WORK UNIT NUMBER		
7. PERFORMING ORGANIZATION NAME(S) AND ADDRESS(ES) <b>Naval Underwater Systems Center, New London, CT, 06320</b>			8. PERFORMING ORGANIZATION REPORT NUMBER <b>TM No. 851103</b>		
9. SPONSORING/MONITORING AGENCY NAME(S) AND ADDRESS(ES) <b>Office of Naval Research</b>			10. SPONSOR/MONITOR'S ACRONYM(S)		
			11. SPONSOR/MONITOR'S REPORT NUMBER(S)		
12. DISTRIBUTION/AVAILABILITY STATEMENT <b>Approved for public release; distribution unlimited</b>					
13. SUPPLEMENTARY NOTES <b>NUWC2015 This technical memorandum consists of the text and vignettes of an invited paper presented at the Underwater Flow Noise session of the 109th Meeting of the Acoustical Society of America held at Austin, Texas on 8-12 April 1985.</b>					
14. ABSTRACT <b>The objective of this paper is to develop a model for calculating the turbulent boundary layer pressure fluctuation transmitted into a layer of viscoelastic material. The theoretical model used here is a plane elastomer layer backed by a rigid plane surface. The other side of the plane surface is exposed to a turbulent flow. The transmitted flow noise received by a rectangular hydrophone embedded in the elastomer layer was calculated for various turbulent boundary layer forcing functions developed by Corcos, and by Chase. The transmitted flow noise was characterized by the frequency spectral density expressed in decibels. Wave-vector spectral densities of various turbulent wall pressures were discussed. Effects of the elastomer layer thickness, material properties and flow conditions on the transmitted noise level are presented.</b>					
15. SUBJECT TERMS <b>turbulent boundary layer pressure; flow noise</b>					
16. SECURITY CLASSIFICATION OF:			17. LIMITATION OF ABSTRACT <b>Same as Report (SAR)</b>	18. NUMBER OF PAGES <b>47</b>	19a. NAME OF RESPONSIBLE PERSON
a. REPORT <b>unclassified</b>	b. ABSTRACT <b>unclassified</b>	c. THIS PAGE <b>unclassified</b>			



851103  
cy001

TM No. 851103

REFERENCE ONLY

NAVAL UNDERWATER SYSTEMS CENTER  
NEW LONDON LABORATORY  
NEW LONDON, CONNECTICUT 06320

Technical Memorandum

CALCULATIONS OF TURBULENT BOUNDARY LAYER (TBL) PRESSURE  
FLUCTUATIONS TRANSMITTED INTO A VISCOELASTIC LAYER

21 June 1985

Prepared by: Sung H. Ko  
Dr. Sung H. Ko  
Submarine Sonar Department

Howard H. Schloemer  
Dr. Howard H. Schloemer  
Submarine Sonar Department

Approved for Public Release; distribution unlimited.

## ABSTRACT

This technical memorandum consists of the text and vignettes of an invited paper presented at the Underwater Flow Noise session of the 109th Meeting of the Acoustical Society of America held at Austin, Texas on 8-12 April 1985. The following abstract was published in the Journal of the Acoustical Society of America, Supplement 1, Vol. 77, Spring 1985.

The objective of this paper is to develop a model for calculating the turbulent boundary layer pressure fluctuation transmitted into a layer of viscoelastic material. The theoretical model used here is a plane elastomer layer backed by a rigid plane surface. The other side of the plane surface is exposed to a turbulent flow. The transmitted flow noise received by a rectangular hydrophone embedded in the elastomer layer was calculated for various turbulent boundary layer forcing functions developed by Corcos, and by Chase. The transmitted flow noise was characterized by the frequency spectral density expressed in decibels. Wave-vector spectral densities of various turbulent wall pressures were discussed. Effects of the elastomer layer thickness, material properties and flow conditions on the transmitted noise level are presented.

## ADMINISTRATIVE INFORMATION

This memorandum was prepared under NUSC Project No. D70011, Program Element No. 62702E, "Advanced Conformal <sup>Submarine</sup> Acoustic Sensor Program - Hydrophone and Arrays," Principal Investigator, Dr. Sung H. Ko (Code 3233). The NUSC ACSAS Program Manager is Dr. Charles H. Sherman (Code 3292). The sponsoring activity is Office of Naval Research, Code 280 (James W. Webster).

The authors of this memorandum are located at New London Laboratory, Naval Underwater Systems Center, New London, Connecticut 06320.

FIGURE 1

Title

Name

Organization

FIGURE 2 (THEORETICAL MODEL)

The model used here is a plane elastomer layer of an infinite extent backed by a rigid surface. The other side of the elastomer layer is exposed to a turbulent flow. In this model the fluid medium is characterized by the fluid density  $\rho_0$  and the speed of sound  $c_0$ . The free stream velocity is denoted by  $U$ . The elastomer is characterized by the Lamé constants  $\lambda$  and  $\mu$ , which are expressed in terms of the Young's modulus  $E$ , the Poisson's ratio  $\sigma$ , and the material density  $\rho_c$ . Both shear and compressional wave speeds in the elastomer can be expressed in terms of these material parameters. The thickness of the elastomer layer is denoted by  $h$ , and  $d$  is the standoff distance from the rigid backing where the transmitted turbulent boundary layer pressure fluctuation sensed by a hydrophone is calculated.

The main results to be presented in this paper are turbulent boundary layer noise reductions, which are given relative to the noise level calculated in the absence of the elastomer layer. Specifically, the turbulent boundary layer noise reduction is the difference between the turbulent noise level calculated in the absence of the elastomer layer and that calculated at a standoff distance in the presence of the elastomer layer.

FIGURE 3 (FREQUENCY SPECTRAL DENSITY)

This slide shows the expression for the frequency spectral density. The capital  $P$  is the turbulent wall pressure, which is a function of the wavenumber, frequency, and flow conditions. The capital  $S$  is the hydrophone function, which is a function of the wavenumber and its geometrical dimension. The capital  $T$  is the transfer function, which is a function of the elastomer material property, wavenumber, and frequency. The formulation of the problem is based on the Corcos model for turbulent boundary layer pressure fluctuations and a theory of elasticity representation for the

elastomer layer to obtain the transfer function. It is obvious that the transfer function would be unity if a layer of elastomer were not present. The capital  $Q$  is the frequency spectral density, which is the noise level calculated in terms of decibels.

**FIGURE 4 (CORCOS MODEL)**

This is a model cross-spectrum of turbulent wall pressure, frequently called the Corcos expression, which has been used when the convective domain is dominant. Here,  $k_x$  and  $k_y$  are the wavenumbers in the flow direction and in the direction normal to the flow on the same plane,  $k_c$  is the convective wavenumber, and  $u_c$  is the convective flow velocity.  $v_*$  is the friction velocity, which is a measure of the intensity of turbulent eddy. In practice,  $v_*$  can be expressed as a function of Reynolds number. As shown here, the turbulent wall pressure is characterized by a wavevector-frequency spectrum.

**FIGURE 5 (BASELINE DATA)**

These are the baseline data used in this study. Before discussing the major results, we would like to go over the parameters needed for their calculations. Note the two columns on the right side of this slide: one is for the point hydrophone and the other is for a finite hydrophone. The stand-off distance is denoted by  $d$  and is equal to zero, which means the hydrophone is embedded at the bottom of the layer. The elastomer layer thickness  $h$  is 3 in. for the point hydrophone and 1-in. for the 2-in. square hydrophone.  $L_x$  and  $L_y$  represent the dimension of a rectangular hydrophone in the flow direction and that in the direction normal to the flow, respectively. The elastomer density  $\rho_c$  is  $1200 \text{ kg/m}^3$ , which is the value for a natural rubber. The loss factor of the elastomer associated with the shear wave speed  $\zeta_s$  is 0.3, and 10 percent of this value is used for the loss factor associated with the compressional wave speed. The shear wave speed  $c_{to}$  is 16.66 m/sec, which is obtained for the natural rubber having the Young's modulus  $10^6 \text{ N/m}^2$ , the density of  $1200 \text{ kg/m}^3$  and the Poisson's ratio of 0.5. The compressional wave speed is 2000 m/sec, which is obtained in a similar way for the natural rubber. The water density

$\rho_0$ , the speed of sound in water  $c_0$  and the free stream velocity  $U$  are self-explanatory. The convective flow velocity used here is 0.6 times the free stream velocity. This number is acceptable only for a relatively high frequency when the displacement thickness is fixed. In general, the convective flow speed increased toward low frequency. The friction velocity is 0.035 times the free stream velocity.

**FIGURE 6** (TBL AT 100 Hz)

These are the calculated results of the Corcos model for the turbulent boundary layer power spectrum as a function of the wavenumber at 100 Hz. In this figure, we can see three different curves. The first curve having a peak value at the center, is the turbulent boundary layer power spectrum as a function of the wavenumber  $k_x$  in the positive direction with the wavenumber  $k_y = 0$ . The peak level is observed where the wavenumber  $k_x$  is equal to the convective wavenumber  $k_c$ . Beyond this peak the level falls off rapidly. The second curve is the wavenumber response in the negative direction of the wavenumber  $k_x$  with  $k_y = 0$ . As can be seen here, this curve decreases very slowly as the wavenumber  $k_x$  increases negatively. The third curve is the wavenumber response as a function of  $k_y$  with  $k_x = 0$ . The reason for having the absolute value of  $k_y$  is that the Corcos expression is symmetrical in the wavenumber  $k_y$ . Note that these three curves describe the Corcos model in a two-dimensional domain.

**FIGURE 7** (TBL AT 500 Hz)

These are the results of the Corcos model similar to those shown in the previous slide. Now, this is the result for 500 Hz instead of 100 Hz. Note that the convective ridge has moved to a higher wavenumber  $k_x$ . General behavior of the Corcos expression at 500 Hz appears to be similar to that at 100 Hz.

**FIGURE 8** (TBL AT 1000 Hz)

These are the results for 1000 Hz. Again, the convective ridge has moved further to a higher wavenumber  $k_x$ .

FIGURE 9 (TBL CURVES FOR COMPARISON)

These are the calculated results of the Corcos expression as a function of the axial wavenumber  $k_x$  for different frequencies. Note that as the frequency increases, the level decreases and the peak level shifts to a higher wavenumber  $k_x$ .

FIGURE 10 (CONTOUR PLOT OF TBL AT 500 Hz)

This is a contour plot of the Corcos model for the normalized turbulent boundary layer power spectrum as a function of the wavenumbers  $k_x$  and  $k_y$  at 500 Hz. These results are the values of contours normalized with respect to the turbulent boundary layer power spectrum at the convective wavenumber  $k_c$  with  $k_y = 0$ . As can be seen in the figure the peak occurs at the wavenumber  $k_x$  equal to 5.0, which is the convective wavenumber. The interval of contour lines is 5 dB. This type of the contour plot is very useful to estimate a maximum contribution for the calculating of the frequency spectral density. These curves describe the Corcos model completely in the two-dimensional domain, where contour lines are relative turbulent boundary layer power spectrum levels.

FIGURE 11 (CONTOUR PLOT OF TBL AT 1000 Hz)

These are the calculated results for the Corcos model at 1000 Hz, which are similar to those presented in the previous slide. The peak level is shown at the wavenumber  $k_x$  equal to 10, which is the value of the convective wavenumber  $k_c$ .

FIGURE 12 (COMPARISON BETWEEN CORCOS AND CHASE MODELS)

The objective of this slide is to present a comparison between the calculated results based on two different models. The turbulent boundary layer power spectrum calculated at 100 Hz using the Corcos model is compared with that calculated at 100 Hz using the Chase convective model. The result of the Corcos model and that of the Chase convective model is denoted by the solid line and the dashed line, respectively. As is shown in the figure, the result of the Corcos model gives a higher level than that of the Chase

convective model. The Chase convective model falls off rapidly toward low wavenumbers. Therefore, Chase has developed a subconvective model, which is a wavenumber white model that defines the level of the turbulent boundary layer power spectrum for low wavenumber region. The wavenumber white model is not discussed here. Remember that this paper is not to discuss the modeling aspect of the turbulent boundary layer power spectrum, but to use a reasonable one for the theoretical calculation of the frequency spectral density, in which case the model chosen here is the one developed by Corcos.

FIGURE 13 (COMPARISON OF TBL AT 500 Hz)

These are the calculated results of both Corcos and Chase convective models similar to those shown in the previous slide. Now, these are the results for 500 Hz instead of 100 Hz. It is shown that general behaviors for both results for 500 Hz are similar to those for 100 Hz.

FIGURE 14 (COMPARISON OF TBL AT 1000 Hz)

This is another comparison between the calculated results of the Corcos model and the Chase convective model.

FIGURE 15 (TRANSFER FUNCTION)

The transfer function for a 3-in. thick layer at three frequencies is shown in this slide. The transfer function is a measure of the wavenumber filtering, and it is a function of the material property, the layer thickness, and the standoff distance. The transfer function will not be discussed here in detail. However, we would like to indicate how it was obtained. The boundary conditions used here are based on the following assumptions. The fluctuating shear stress exerted by the turbulent boundary layer is assumed to be negligible; and thus the tangential stress vanishes at the interface between the fluid flow and the elastomer layer. At this interface the force acting in the normal direction must be balanced. The elastomer layer is perfectly bonded to the rigid backing, and thus no particle motions are allowed in both normal and tangential directions at the interface between the elastomer layer and the backing material. That is,

both normal and tangential displacements of the particle become zero at this interface. In this figure the peak values are observed at the corresponding shear wavenumbers for different frequencies. The wave propagates in the elastomer layer below the shear wavenumber, and decays in the direction normal to the layer surface toward the rigid backing above the shear wavenumber. These decaying waves are called evanescent waves. It is shown in the figure that these evanescent waves fall off very rapidly, as the wavenumber increases.

#### FIGURE 16 (HYDROPHONE FUNCTION)

An averaged sensitivity for the rectangular hydrophone is shown on top. The sensitivity for the circular hydrophone is shown at the bottom. Here,  $J_1(ka)$  is the Bessel function of the order one with argument  $ka$ .  $k$  is the wavenumber in the radial direction. Remember that the sensitivity of the point hydrophone is equal to one. That is, both the rectangular hydrophone function and the circular hydrophone function approach unity as  $k_x L_x$  and  $k_y L_y$ , and  $ka$  approach zero.

#### FIGURE 17 (VARIOUS HYDROPHONE FUNCTIONS)

This slide shows a comparison between three different sensitivity curves. The solid line is the 2-in. square hydrophone sensitivity calculated using the formula shown in the previous slide. The dashed line is the hydrophone sensitivity calculated for a 2-in. diameter circular hydrophone. The broken line is the sensitivity for the square hydrophone having the same area as the circular hydrophone.

#### FIGURE 18 (FREQUENCY SPECTRAL DENSITY)

In this figure the solid line is the frequency spectral density calculated using the square hydrophone, the transfer function for a 1-in. thick layer of the natural rubber and the turbulent boundary layer power spectrum developed by Corcos. The frequency spectral density calculated for the flush-mounted point hydrophone is given by the dashed line. That is, the dashed line is the turbulent boundary layer pressure fluctuation

calculated on the rigid surface in the absence of the elastomer layer using the Corcos model. The difference between these two results is the reduction of the turbulent boundary layer pressure fluctuations, which may be simply called the turbulent boundary layer noise reduction. The power spectral level shown here is expressed in decibels based on  $\mu\text{Pa}^2/\text{Hz}$ .

FIGURE 19 (VARIATION OF LAYER THICKNESS;  $h$ )

These are the results of the turbulent boundary layer noise reductions calculated for various layer thickness using a point hydrophone. The top horizontal line represents the case of flush mounted point hydrophone. As can be seen here, more noise reduction is achieved as the layer thickness increases. At this point, we would like you to keep in mind that the results to be presented in the forthcoming five slides are also calculated for the point hydrophone.

FIGURE 20 (VARIATION OF STANDOFF DISTANCE;  $d$ )

We now see the effect of the standoff distance on the noise reduction. The elastomer layer thickness here is 3 in. If the standoff distance is 3 in., no noise reduction is achieved. However, if we look at a point which is 1-in. away from the flow surface; that is,  $d=2$  in., we see some noise reduction. It is shown in the figure that as the standoff distance decreases, more noise is attenuated for a given layer thickness.

FIGURE 21 (EFFECT OF LOSS FACTOR;  $\zeta_s$ )

These are the results for various loss factors. As seen in the figure more noise is attenuated as the loss factor  $\zeta_s$  increases except for low frequency. Note that the noise reduction approaches an asymptotic value for high frequency as the value of  $\zeta_s$  increases.

FIGURE 22 (EFFECT OF SHEAR WAVE SPEED;  $c_{to}$ )

This is the effect of the shear wave speed on the noise reduction. As seen in the figure, more noise is attenuated for high frequency, as the

shear wave speed decreases. However, for low frequency, noise is attenuated less as the value of  $c_{to}$  decreases.

FIGURE 23 (EFFECT OF FREE STREAM VELOCITY;  $U$ )

We now see the calculated results for various free stream velocities. As seen in the figure, noise is attenuated less as the free stream velocity of the fluid flow becomes larger.

FIGURE 24 (EFFECT OF LAYER THICKNESS;  $h$ )

These are the noise reduction curves plotted as a function of the elastomer layer thickness for four different frequencies at 20 knots. The noise is reduced more as the thickness increases for a given frequency or as the frequency increases for a given layer thickness.

FIGURE 25 (RELEVANT FUNCTIONS AT 500 Hz)

These are the functions to be used for the calculation of the turbulent boundary layer pressure fluctuations sensed by a 2-in. square hydrophone embedded in the elastomer layer. In this figure the solid line is the hydrophone function, the dashed line is the transfer function at 500 Hz, and the broken line is the turbulent boundary layer power spectrum at 500 Hz calculated using the Corcos model. Finally, the remaining line is the product of these three functions, which is the integrand to be used for calculations.

FIGURE 26 (RELEVANT FUNCTIONS AT 1000 Hz)

These are similar results for 1000 Hz. The product line of three functions at 1000 Hz is much lower than that at 500 Hz.

FIGURE 27 (EFFECT OF HYDROPHONE SIZE;  $L_x = L_y$ )

These are the calculated results of the turbulent boundary layer noise reduction for various sizes of square hydrophones embedded in a 1-in. thick

layer. The dashed line is the result of the point hydrophone. As can be seen in this figure the noise is attenuated more as the size of the square hydrophone increases.

FIGURE 28 (EFFECT OF LAYER THICKNESS;  $h$ )

This slide shows the effect of the layer thickness for the 2-in. square hydrophone on the noise reduction. The solid line is the result for 500 Hz, and the dashed line is the result for 1000 Hz. As shown in this figure, as the thickness increases more noise is reduced for both frequencies. It is also shown that for a given thickness more noise is attenuated as the frequency increases. Note that substantial reductions are observed at zero elastomer layer thickness for both frequencies. These noise reductions are mainly due to the spatial averaging of the 2-in. square hydrophone. Also note that the rate of change of the noise reduction is significant up to the layer thickness of 2 in. However, beyond the layer thickness of 2 in., the noise reduction is less noticeable.

FIGURE 29 (EFFECT OF  $L_x$  FOR  $L_y = 0.5$  in.)

This slide shows the effect of the hydrophone dimension in the flow direction for a fixed hydrophone dimension in the direction normal to the flow direction. For a one inch thick layer the noise is reduced more as the  $L_x$  dimension increases for a given value of  $L_y$ , and as the frequency increases for given values of  $L_x$  and  $L_y$ . Notice that for the case where the dimension of  $L_y$  is less than the dimension of  $L_x$  noise is less reduced. Therefore, it is advantageous to use a rectangular hydrophone such that the dimension of  $L_x$  be larger than that of  $L_y$ . Specifically, more noise is reduced using a rectangular hydrophone than using a square hydrophone if the area of the hydrophone is given equal.

FIGURE 30 (CONCLUSION....POINT HYDROPHONE)

Based on a limited number of calculations, the following conclusions are drawn:

The turbulent boundary layer noise reduction is controlled by the elastomer material property, the elastomer layer thickness, the standoff distance, and the free stream velocity.

The turbulent boundary layer noise reductions increase when the elastomer layer thickness  $h$  and the loss factor  $\zeta_s$  are increased, and when the standoff distance  $d$  and the free stream velocity  $U$  are decreased.

As the shear wave speed  $c_{to}$  increases, the turbulent boundary layer noise reduction increases for low frequency and decreases for high frequency.

FIGURE 31 (CONCLUSION....FINITE HYDROPHONE)

This slide shows a list of conclusions pertinent to finite hydrophones. The turbulent boundary layer noise decreases as the size of the square hydrophone increases, which is mainly attributed to the spatial averaging of the hydrophone. If the area of a rectangular hydrophone is equal to the area of a square hydrophone, greater noise reduction is obtained when the rectangular hydrophone is used provided the dimension of  $L_x$  is greater than  $L_y$ . The conclusions drawn for the point hydrophone are also valid for finite hydrophones.



# **CALCULATIONS OF TURBULENT BOUNDARY LAYER (TBL) PRESSURE FLUCTUATIONS TRANSMITTED INTO A VISCOELASTIC LAYER**

**Sung H. Ko  
and  
Howard H. Schloemer**

**Department of the Navy  
Naval Underwater Systems Center  
New London, Connecticut 06320**

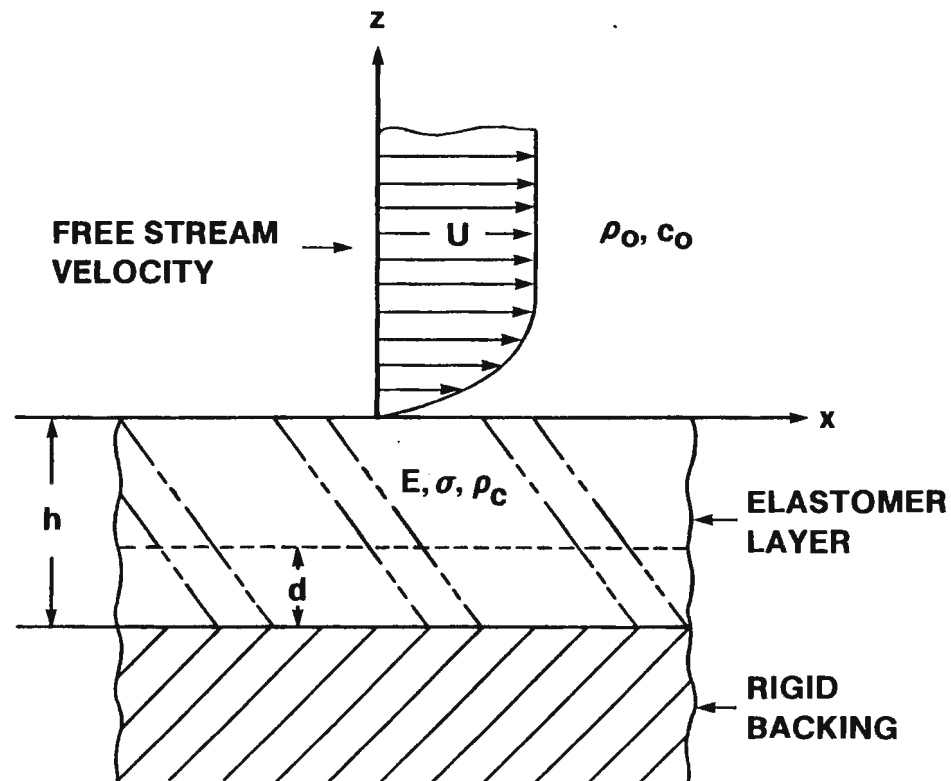
L50342aA

FIGURE 1

TM NO. 851103



## THEORETICAL MODEL



L4873b

FIGURE 2



## **FREQUENCY SPECTRAL DENSITY**

$$Q(\omega) = \iint S(\vec{k}) T(\vec{k}; \omega) P(\vec{k}; \omega) d^2 \vec{k}$$

**WHERE**

$P(\vec{k}; \omega)$  = TBL WAVE NUMBER-FREQUENCY SPECTRAL DENSITY (A FORCING FUNCTION)

$S(\vec{k})$  = HYDROPHONE FUNCTION

$T(\vec{k}; \omega)$  = TRANSFER FUNCTION

L50342bA

FIGURE 3



## CORCOS MODEL

$$P(\vec{k}, \omega) = \frac{a_0 \rho_0^2 v_*^4}{\pi^2 \omega} \left\{ \frac{\alpha_1 k_c}{(k_x - k_c)^2 + (\alpha_1 k_c)^2} \right\} \\ \times \left\{ \frac{\alpha_3 k_c}{k_y^2 + (\alpha_3 k_c)^2} \right\}$$

$$\vec{k} = k_x \vec{i} + k_y \vec{j}$$

$$k_c = \omega / u_c$$

$v_*$  = FRICTION VELOCITY  
(FUNCTION OF REYNOLDS NUMBER)

$$a_0 = a_+ (1 + \gamma)$$

$$\alpha_1 = 0.09$$

$$\alpha_3 = 7 \alpha_1$$

$$a_+ = 0.766$$

$$\gamma = 0.389$$



## BASELINE DATA

	POINT PHONE	FINITE PHONE
STAND-OFF DISTANCE	$d = 0$ in.	●
ELASTOMER LAYER THICKNESS	$h = 3$ in.	$h = 1$ in.
HYDROPHONE SIZE	$L_x = L_y = 0$	$L_x = L_y = 2$ in.
ELASTOMER DENSITY	$\rho_c = 1200$ kg/m <sup>3</sup>	●
LOSS FACTOR OF ELASTOMER	$\zeta_s = 0.3$	●
SHEAR WAVE SPEED	$c_{to} = 16.66$ m/s	●
COMPRESSIONAL WAVE SPEED	$c_{lo} = 2000$ m/s	●
WATER DENSITY	$\rho_o = 1000$ kg/m <sup>3</sup>	●
SOUND SPEED IN WATER	$c_o = 1500$ m/s	●
FREE STREAM VELOCITY	$U = 20$ kts	●
CONVECTIVE FLOW VELOCITY	$U_c = 0.6U$	●
FRICTION VELOCITY	$v_* = 0.035U$	●

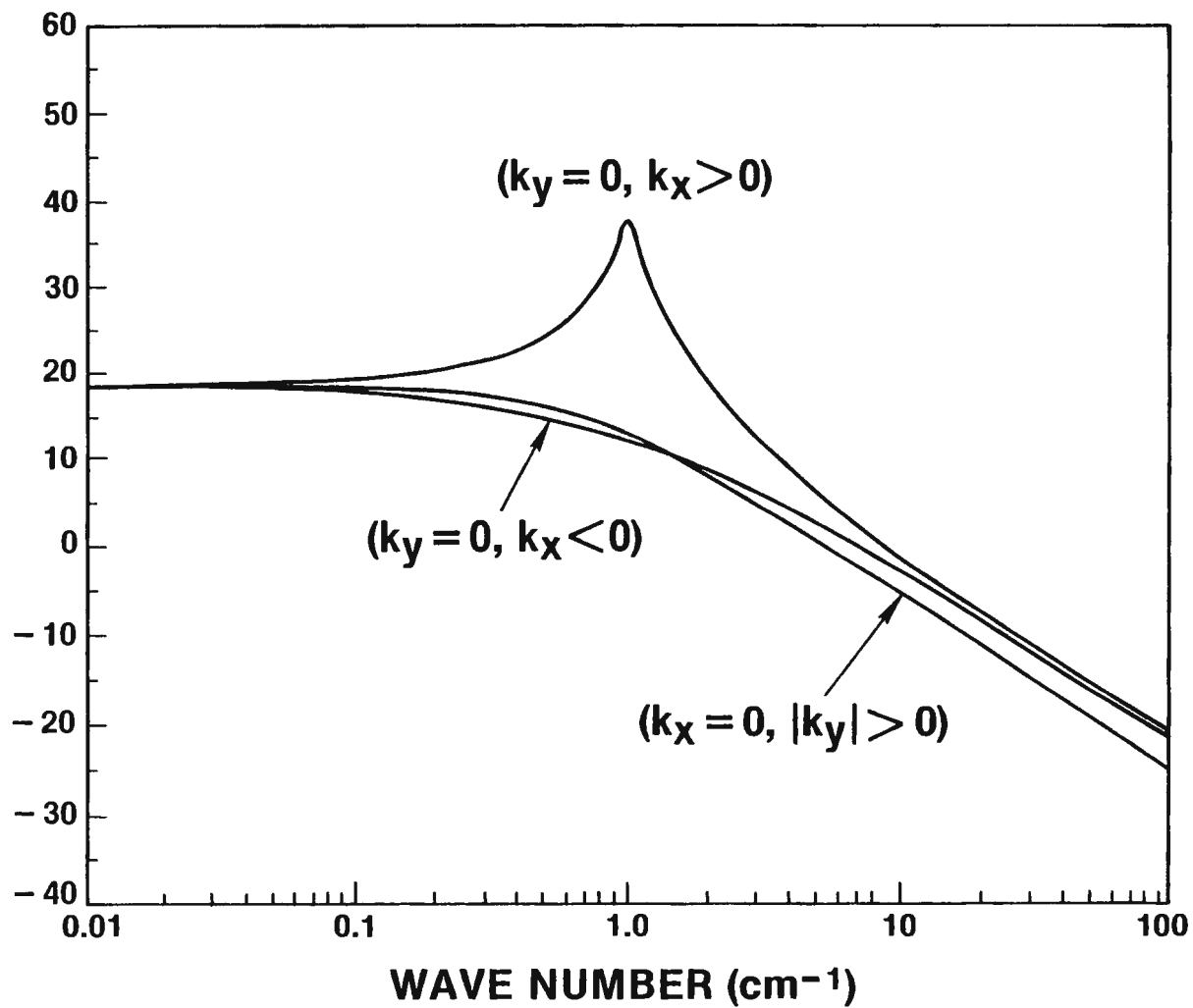
L50342cA

FIGURE 5



TBL POWER SPECTRUM  
(dB//((dynes/cm<sup>2</sup>)<sup>2</sup>·cm<sup>2</sup>·sec)

## WAVE NUMBER RESPONSE AT 100 Hz

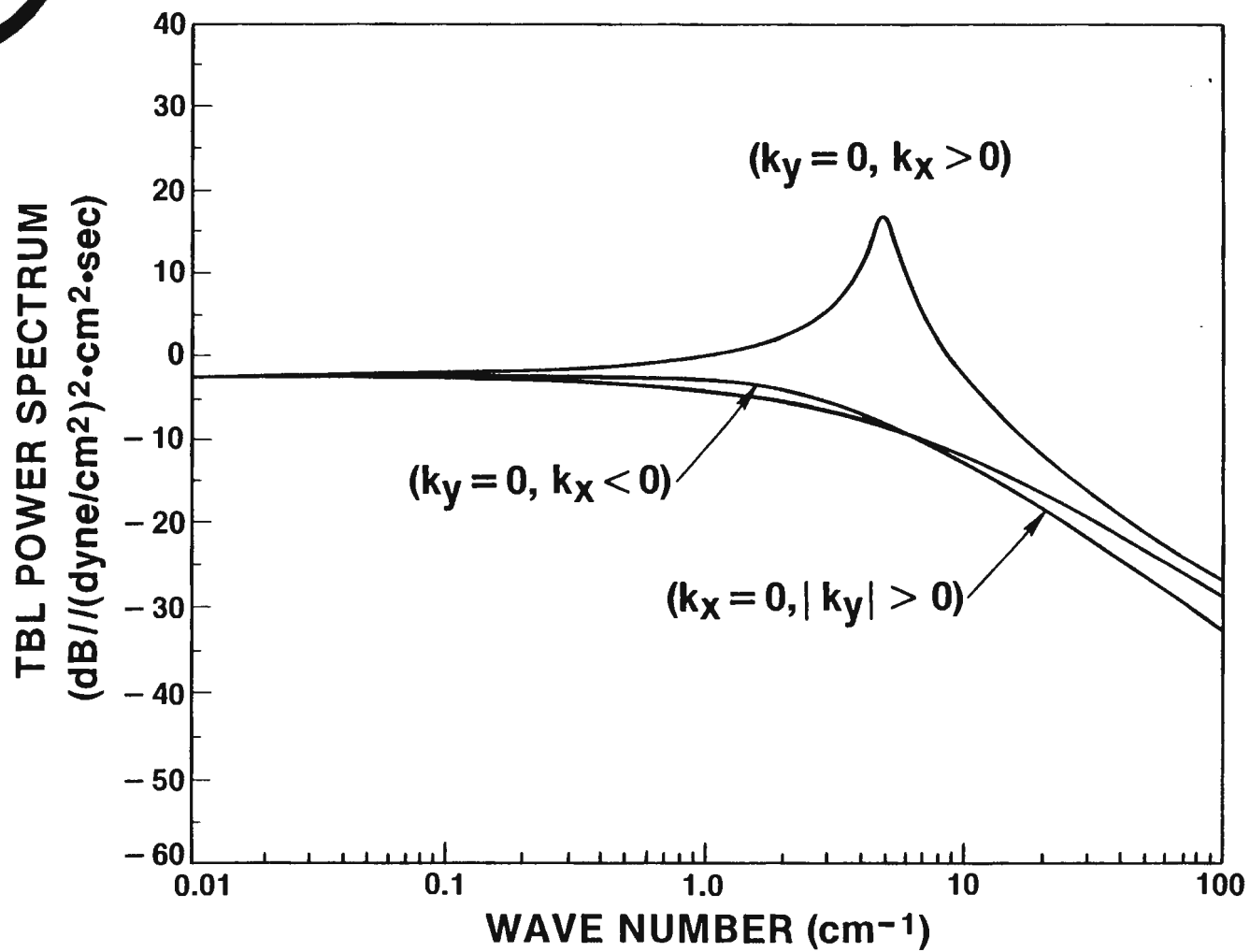


L4873IP

FIGURE 6



## WAVE NUMBER RESPONSE AT 500 Hz



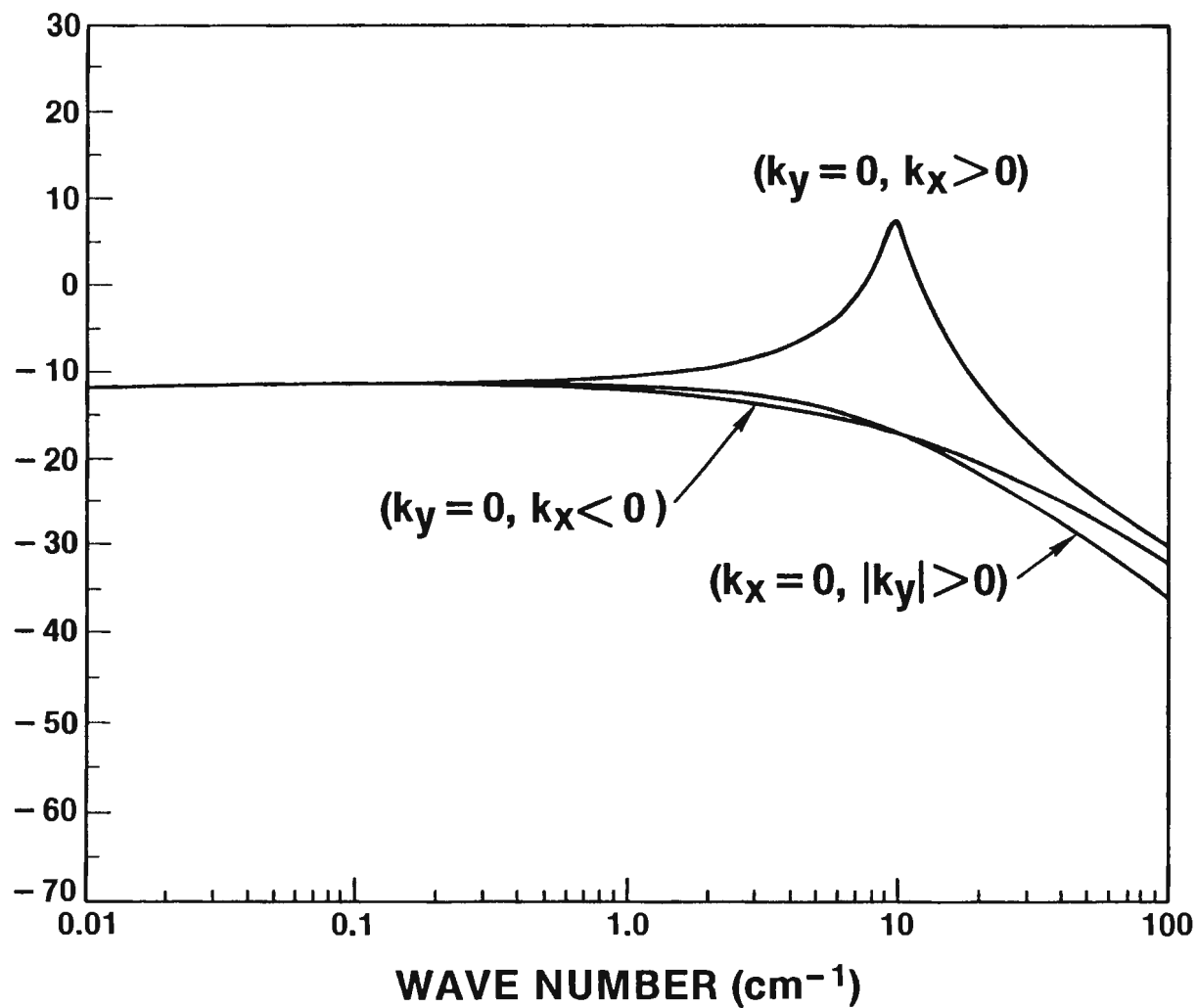
L4873hP

FIGURE 7



TBL POWER SPECTRUM  
(dB//((dynes/cm<sup>2</sup>)<sup>2</sup>·cm<sup>2</sup>·sec)

## WAVE NUMBER RESPONSE AT 1000 Hz

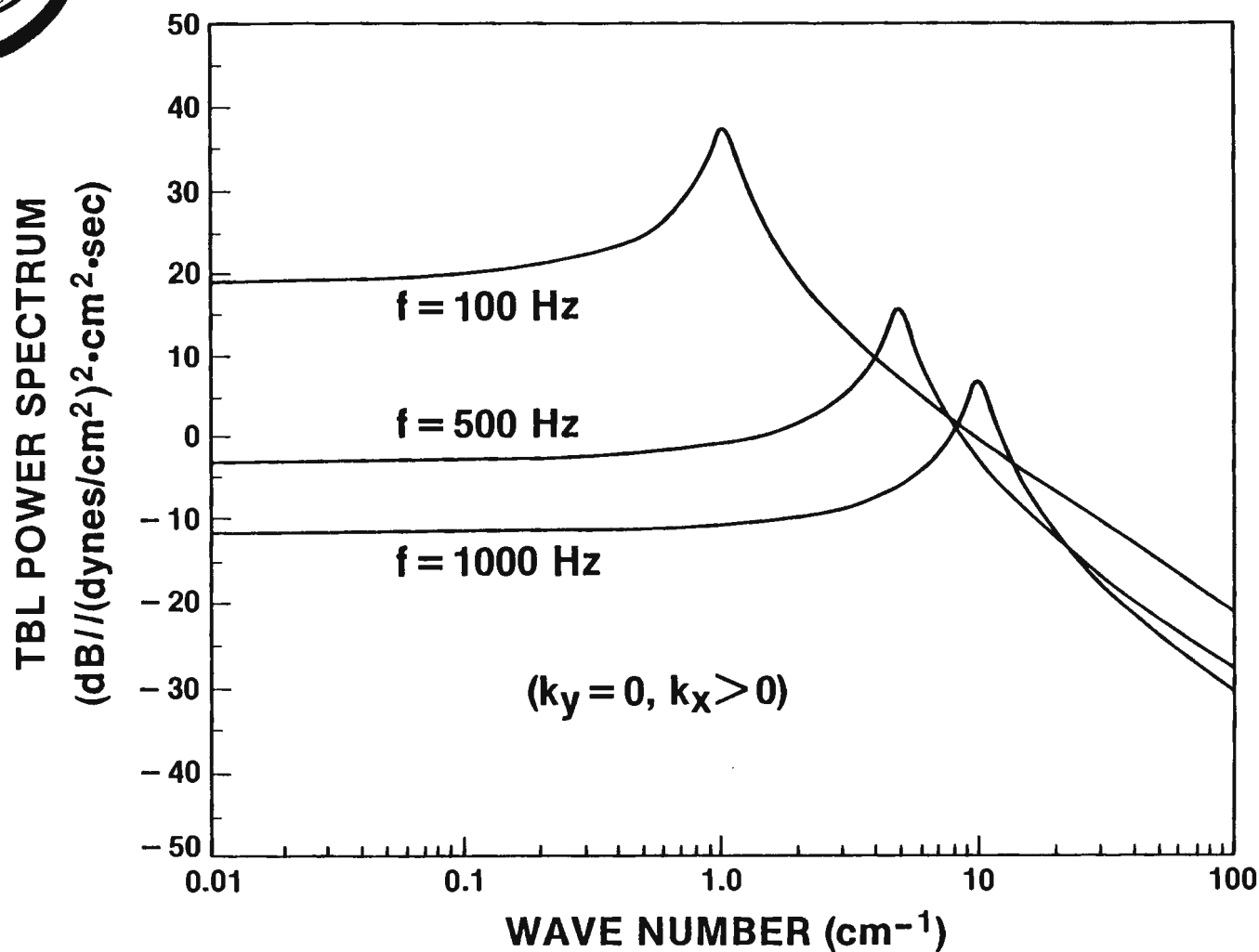


L4873kP

FIGURE 8



## WAVE NUMBER RESPONSES AT DIFFERENT FREQUENCIES

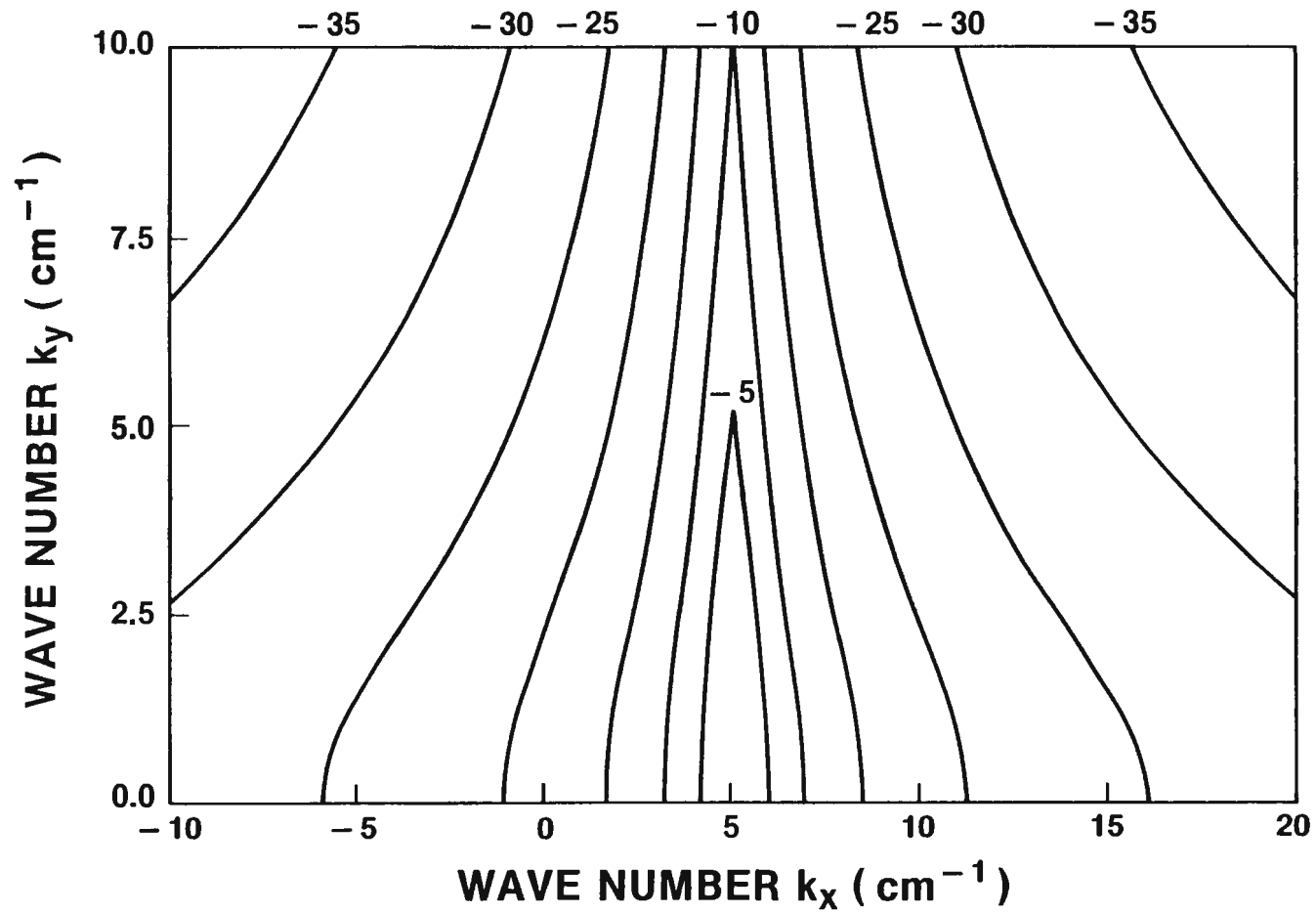


L4873gP

FIGURE 9



## CONTOUR PLOT FOR TBL FUNCTION (500 Hz)

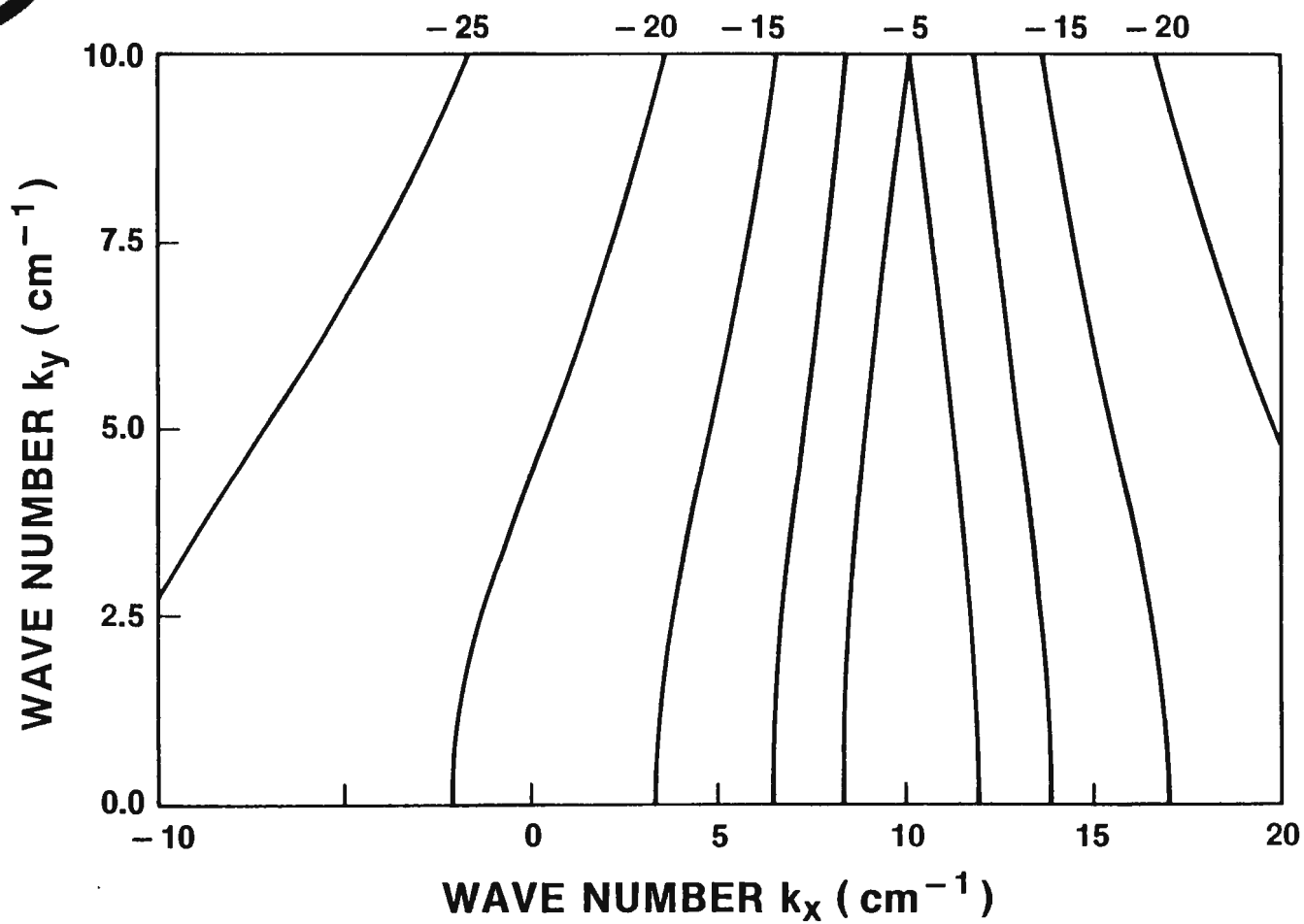


L50342sA

FIGURE 10



## CONTOUR PLOT FOR TBL FUNCTION (1000 Hz)



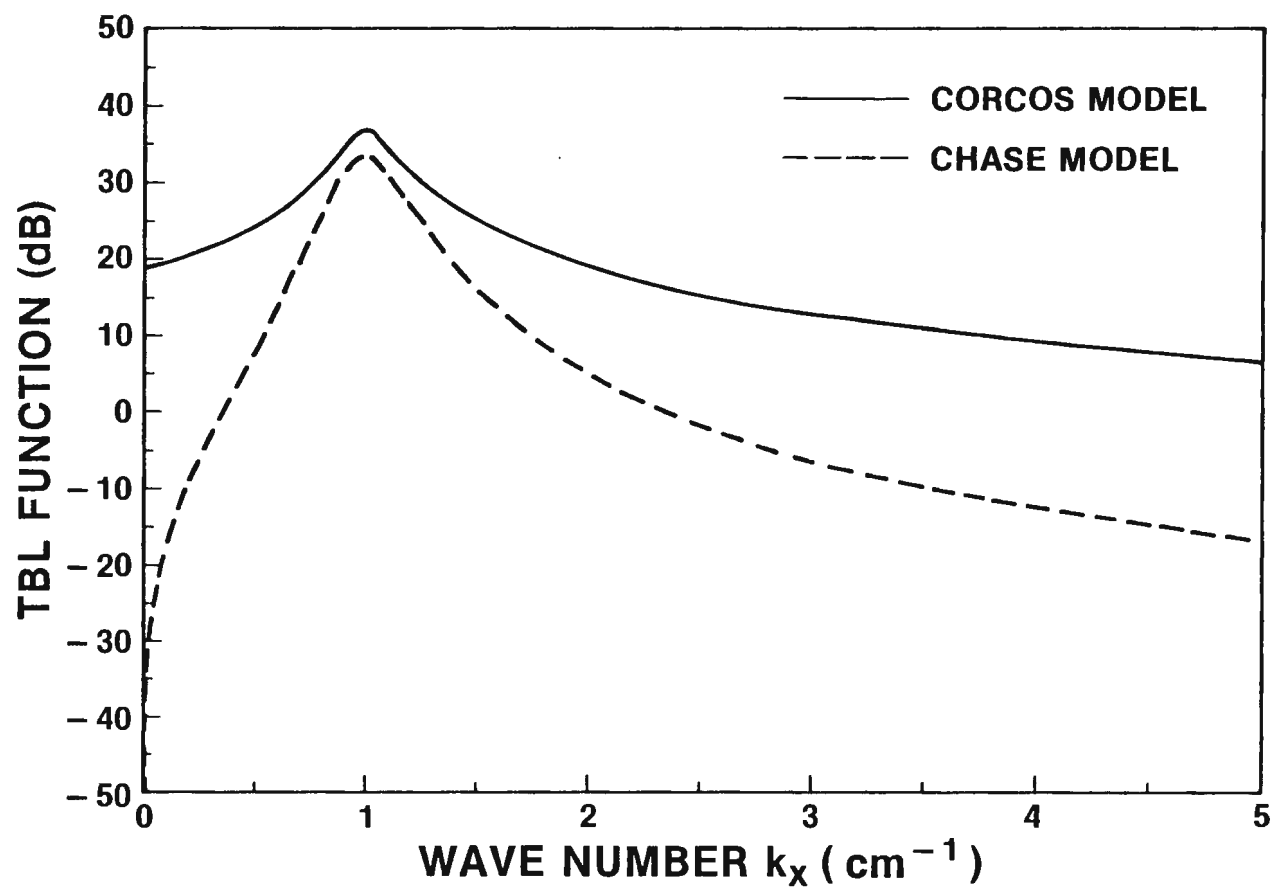
L50342rA

FIGURE 11

TM NO. 851103



## TBL FUNCTION AT 100 Hz

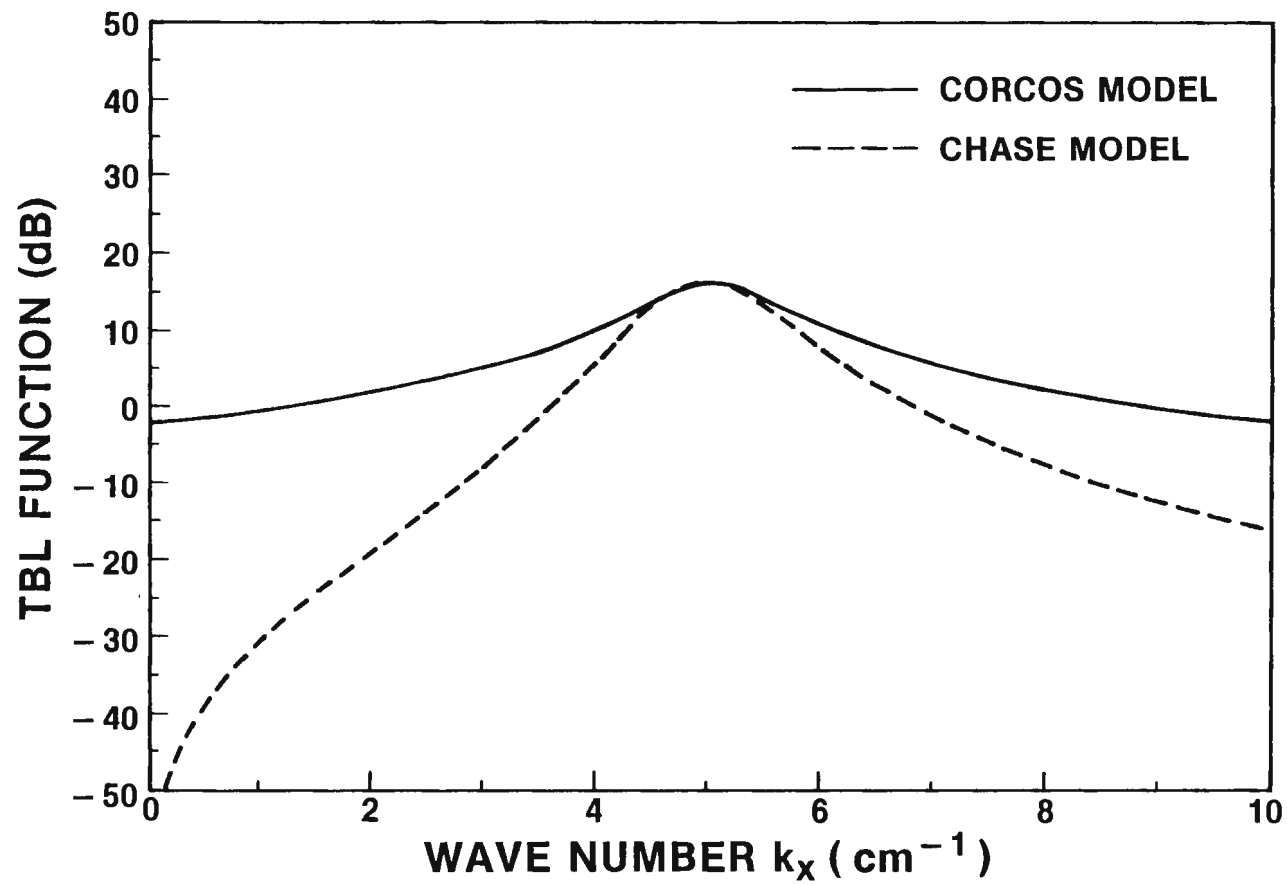


L50342jA

FIGURE 12



## TBL FUNCTION AT 500 Hz

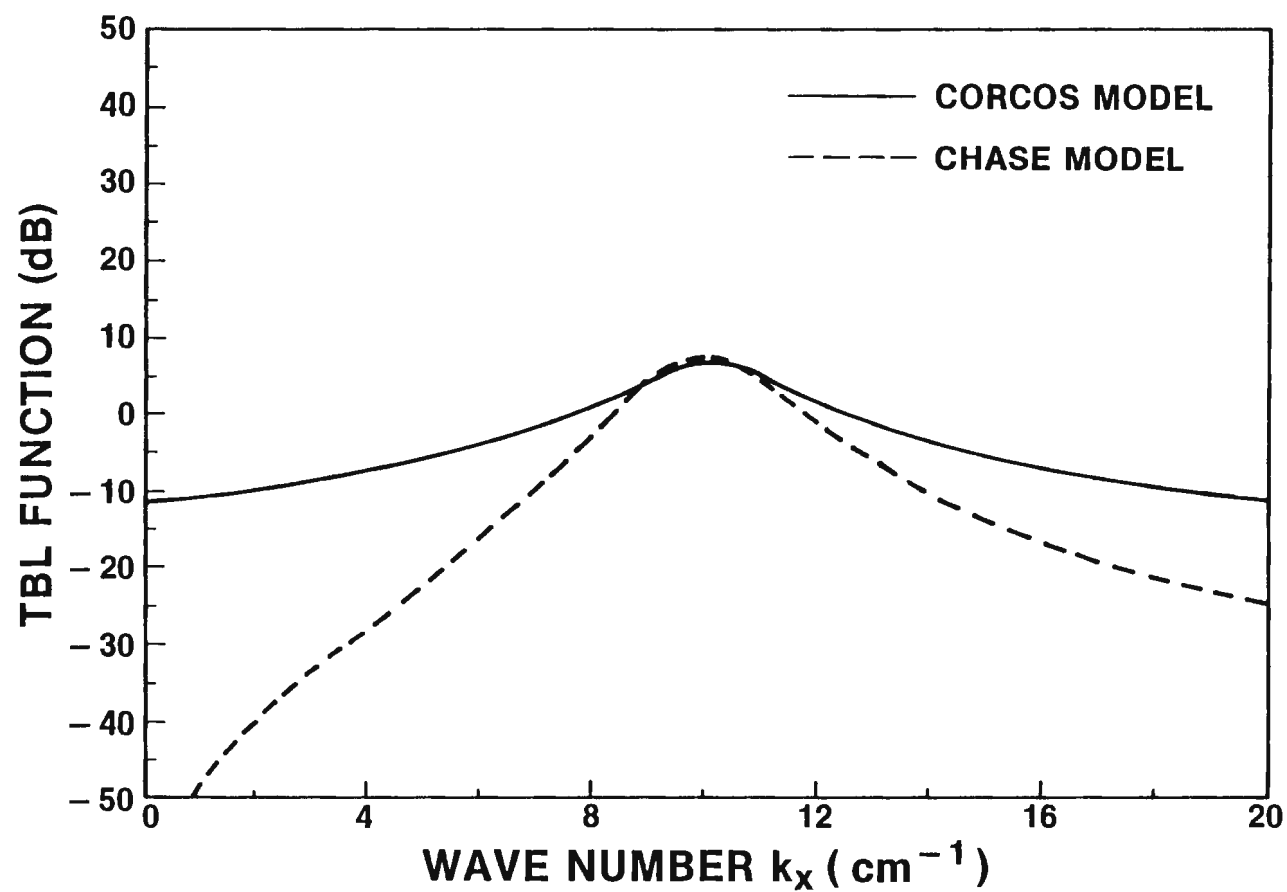


L50342KA

FIGURE 13



## TBL FUNCTION AT 1000 Hz

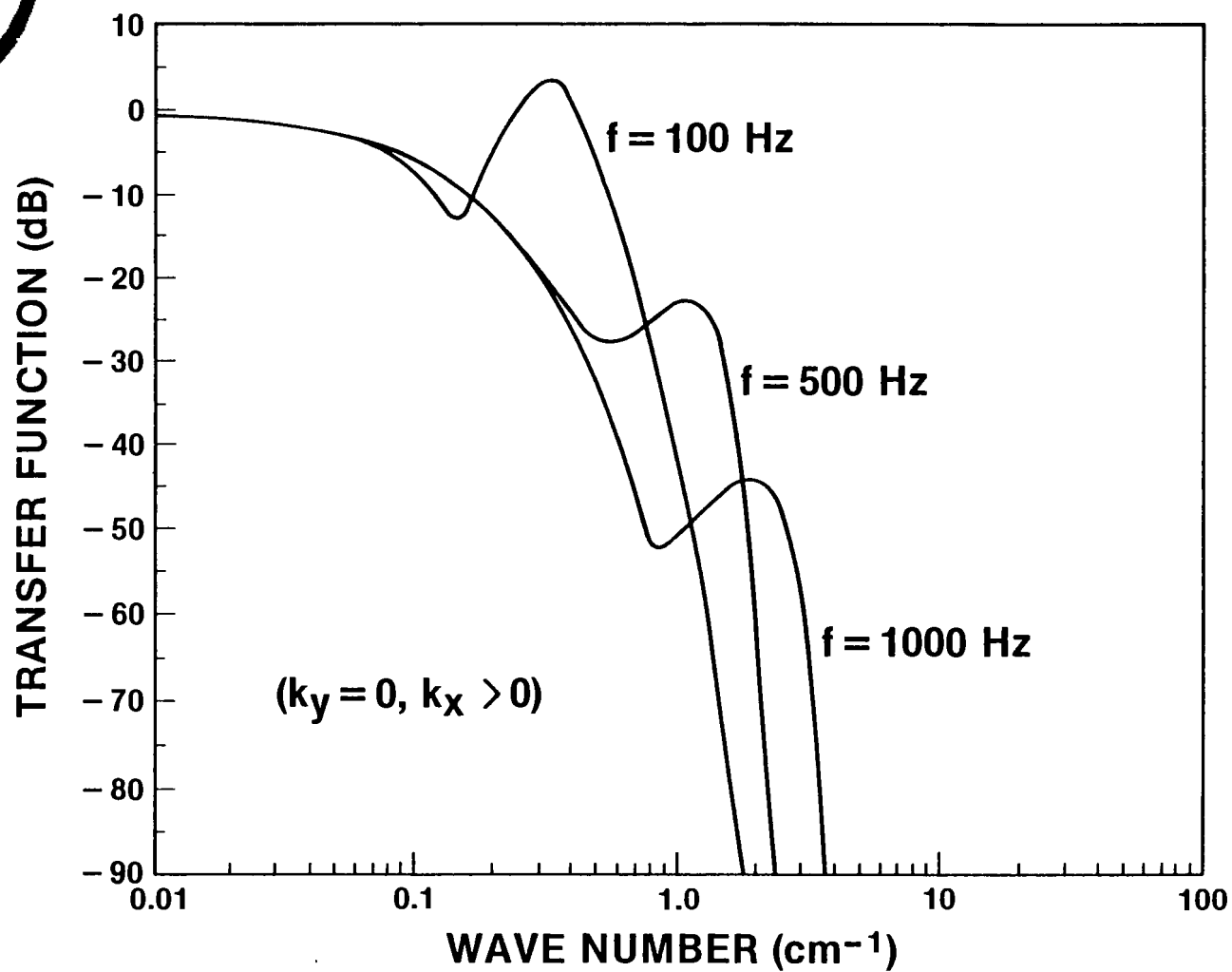


L503421A

FIGURE 14



## TRANSFER FUNCTION



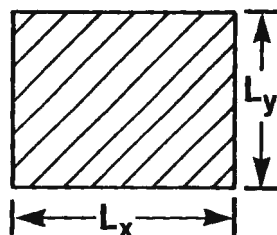
L4873P

FIGURE 15



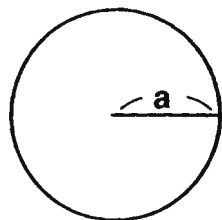
## HYDROPHONE FUNCTIONS

- RECTANGULAR HYDROPHONE



$$S(k_x L_x, k_y L_y) = \left( \frac{\sin(k_x L_x / 2)}{(k_x L_x / 2)} \cdot \frac{\sin(k_y L_y / 2)}{(k_y L_y / 2)} \right)^2$$

- CIRCULAR HYDROPHONE



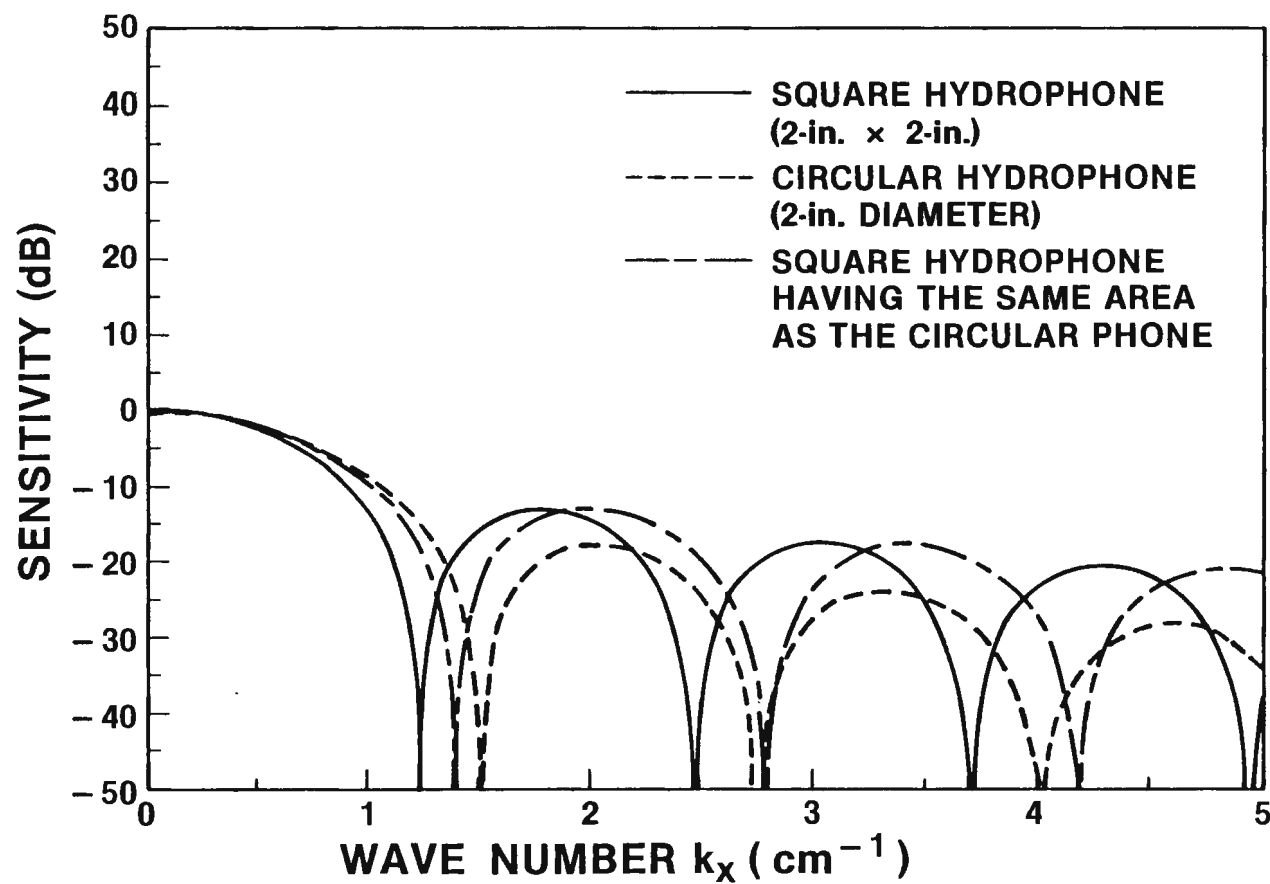
$$S(ka) = \left( \frac{2J_1(ka)}{ka} \right)^2$$

L50342dA

FIGURE 16



## HYDROPHONE FUNCTIONS

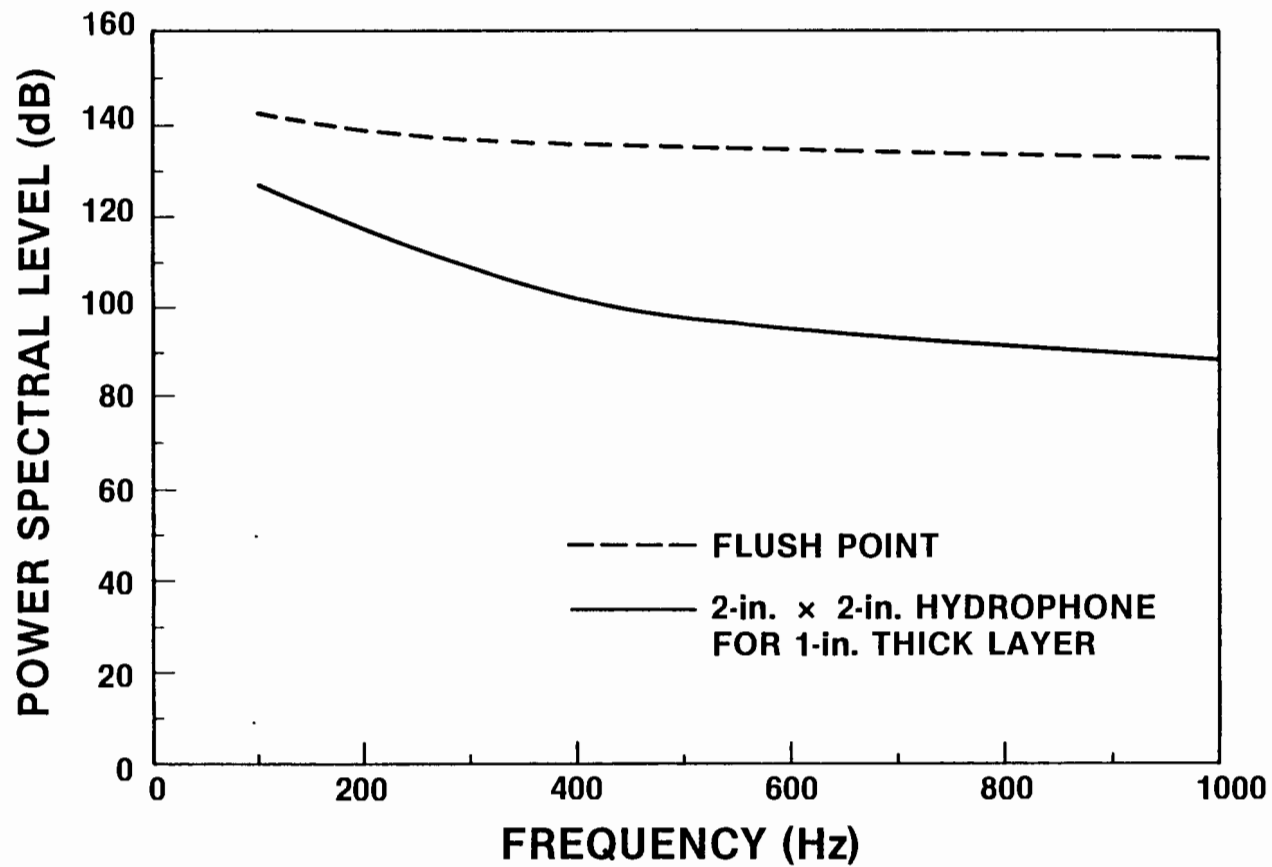


L50342iA

FIGURE 17



## FREQUENCY SPECTRAL DENSITY

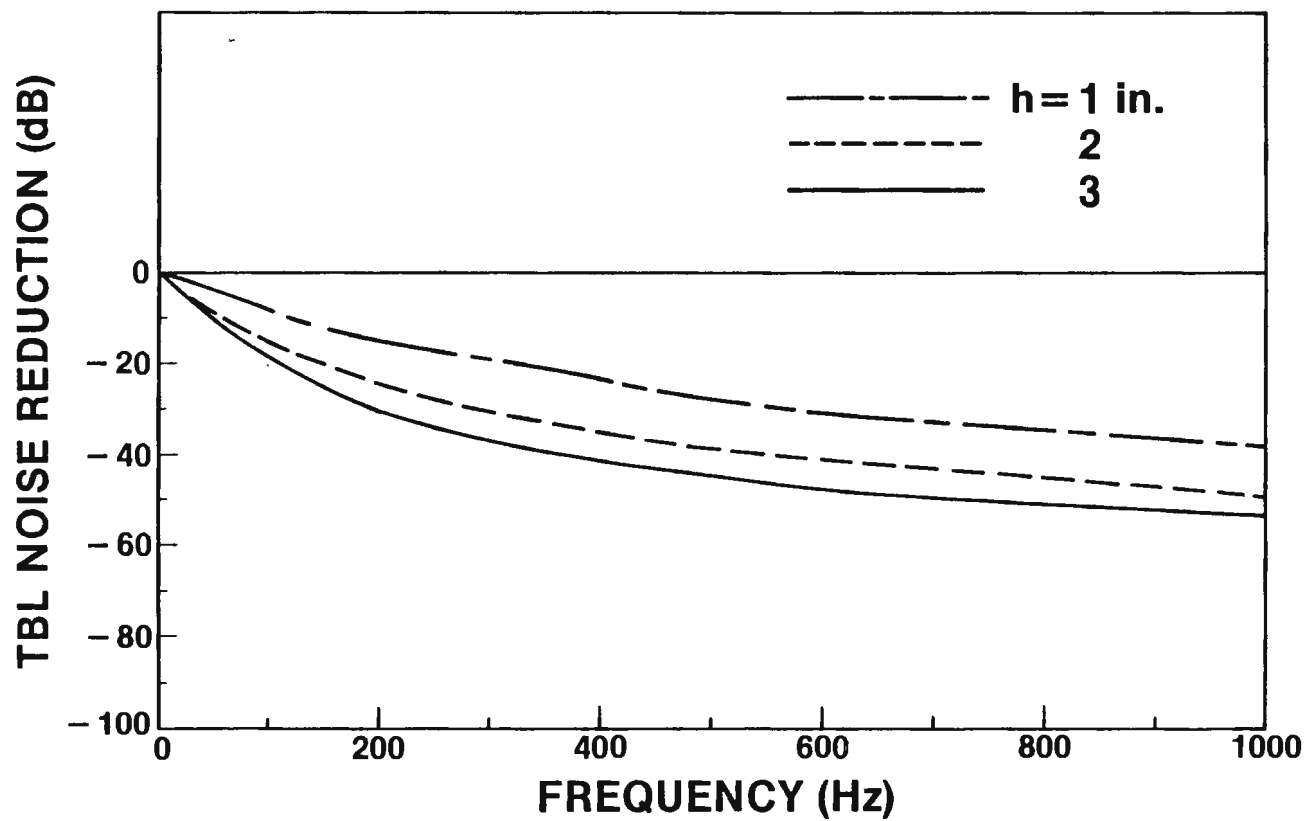


L50342pA

FIGURE 18



## EFFECT OF ELASTOMER LAYER THICKNESS (h)

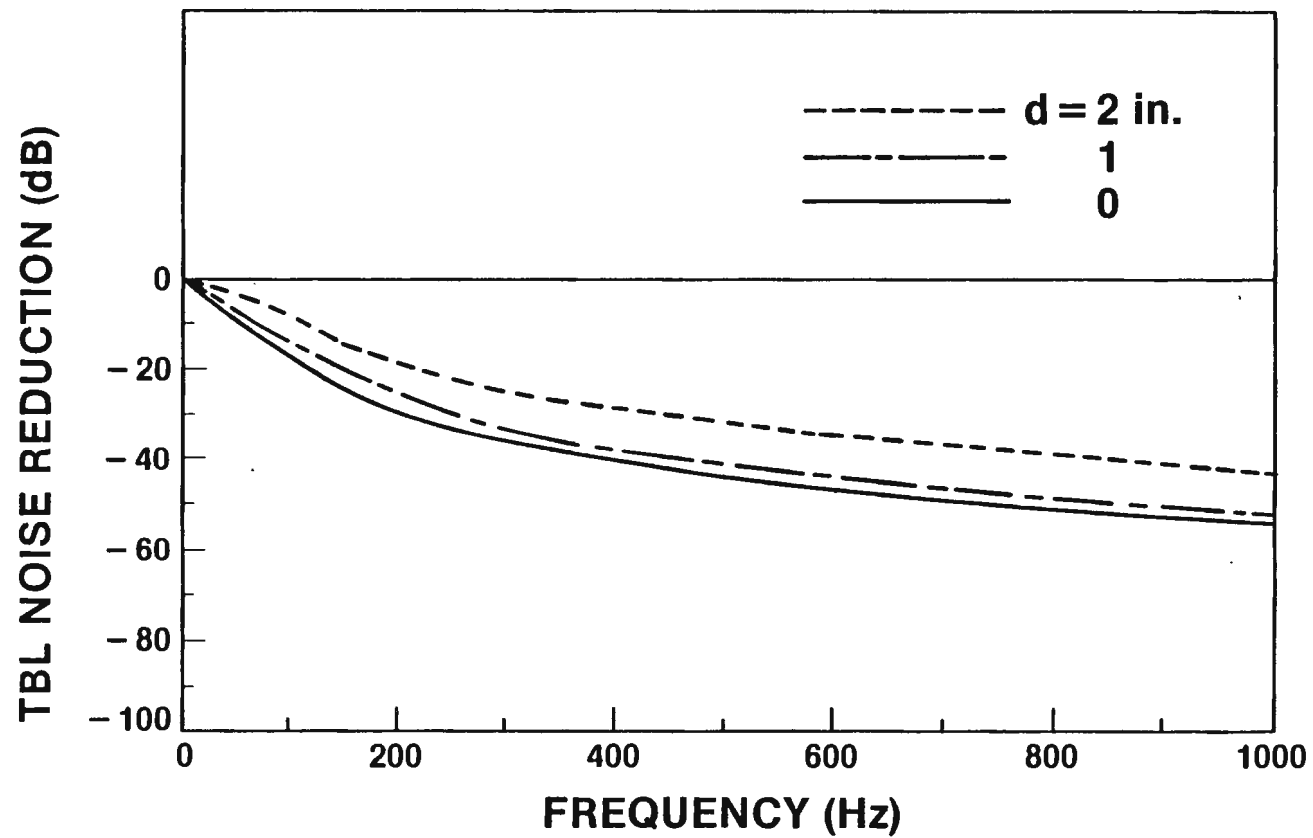


L4873dP

FIGURE 19



## EFFECT OF STAND-OFF DISTANCE (d)

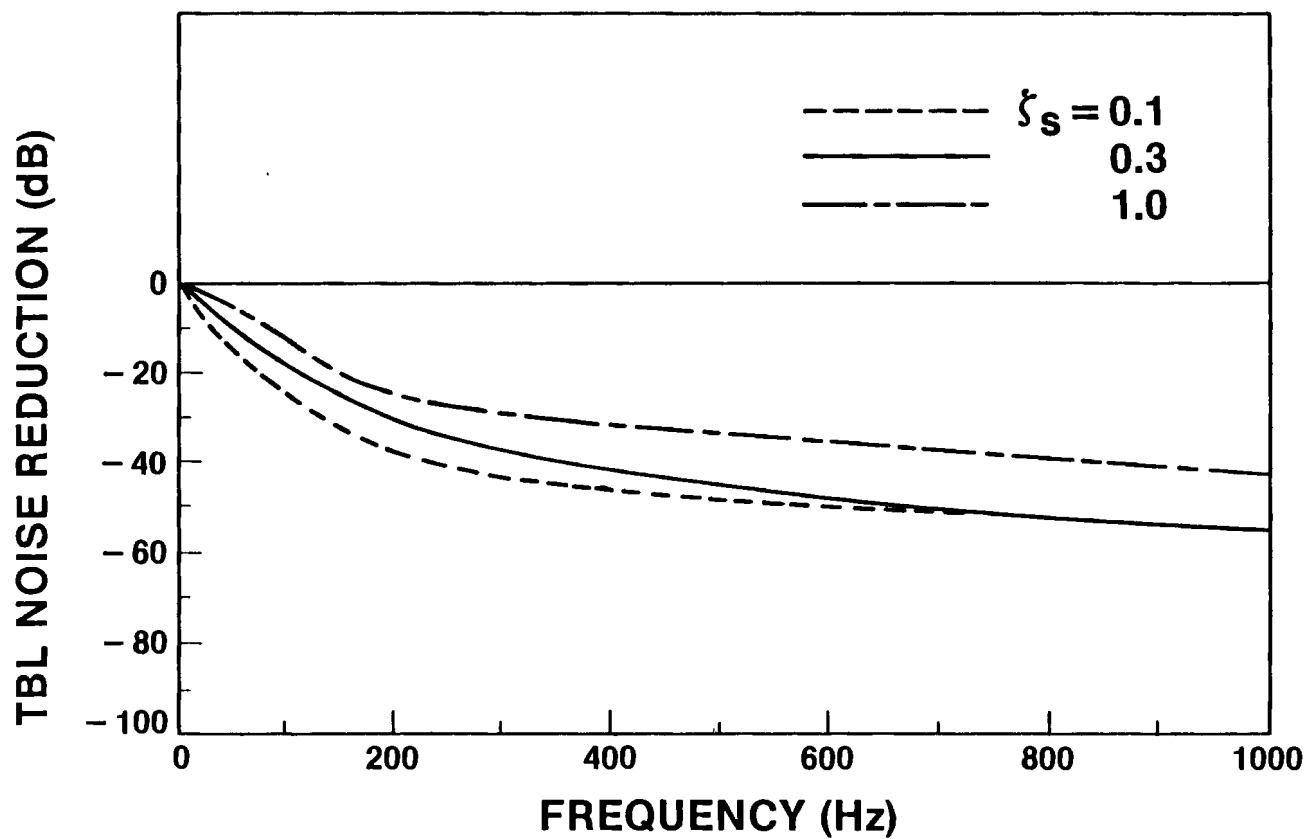


L4873fP

FIGURE 20



## EFFECT OF LOSS FACTOR ( $\xi_s$ )

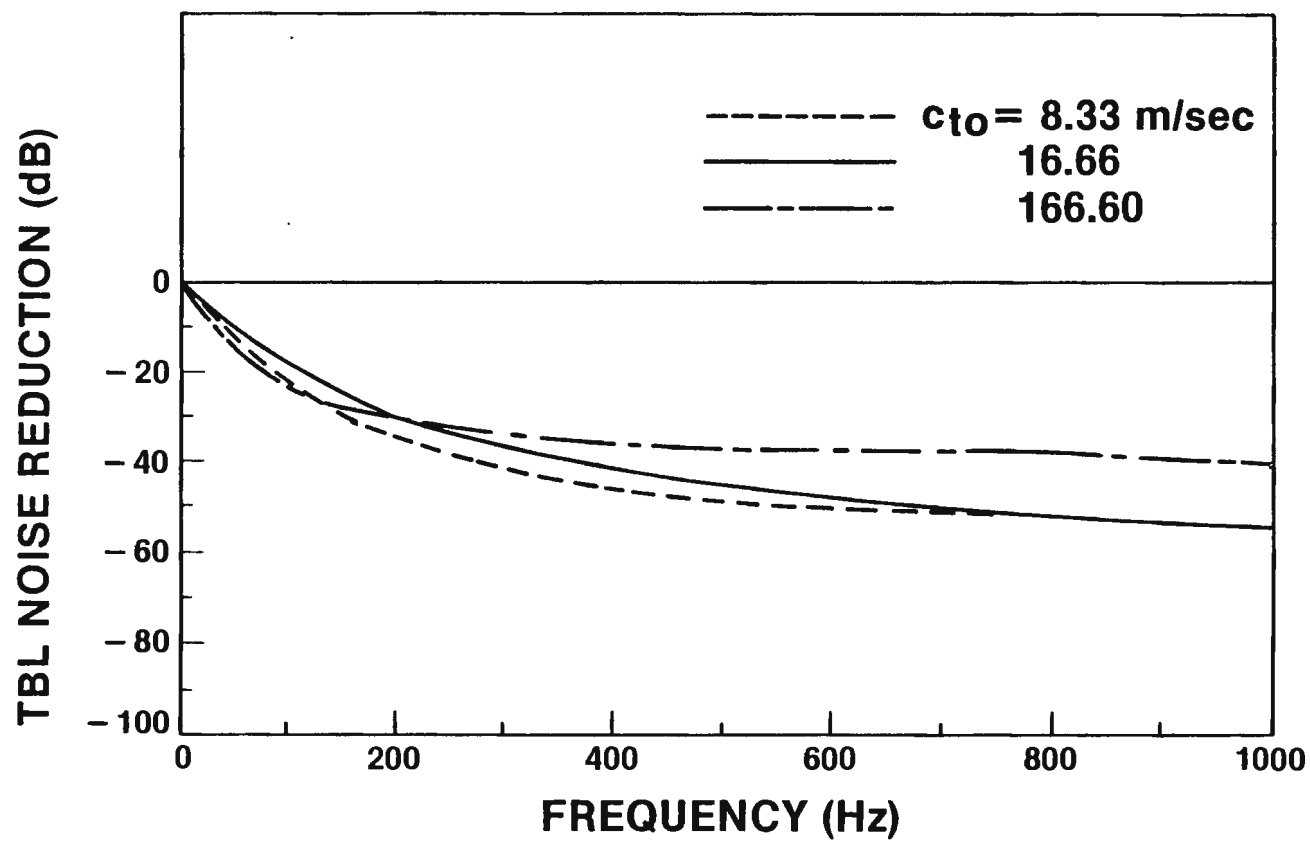


L4873bP

FIGURE 21



## EFFECT OF SHEAR WAVE SPEED ( $c_{to}$ )

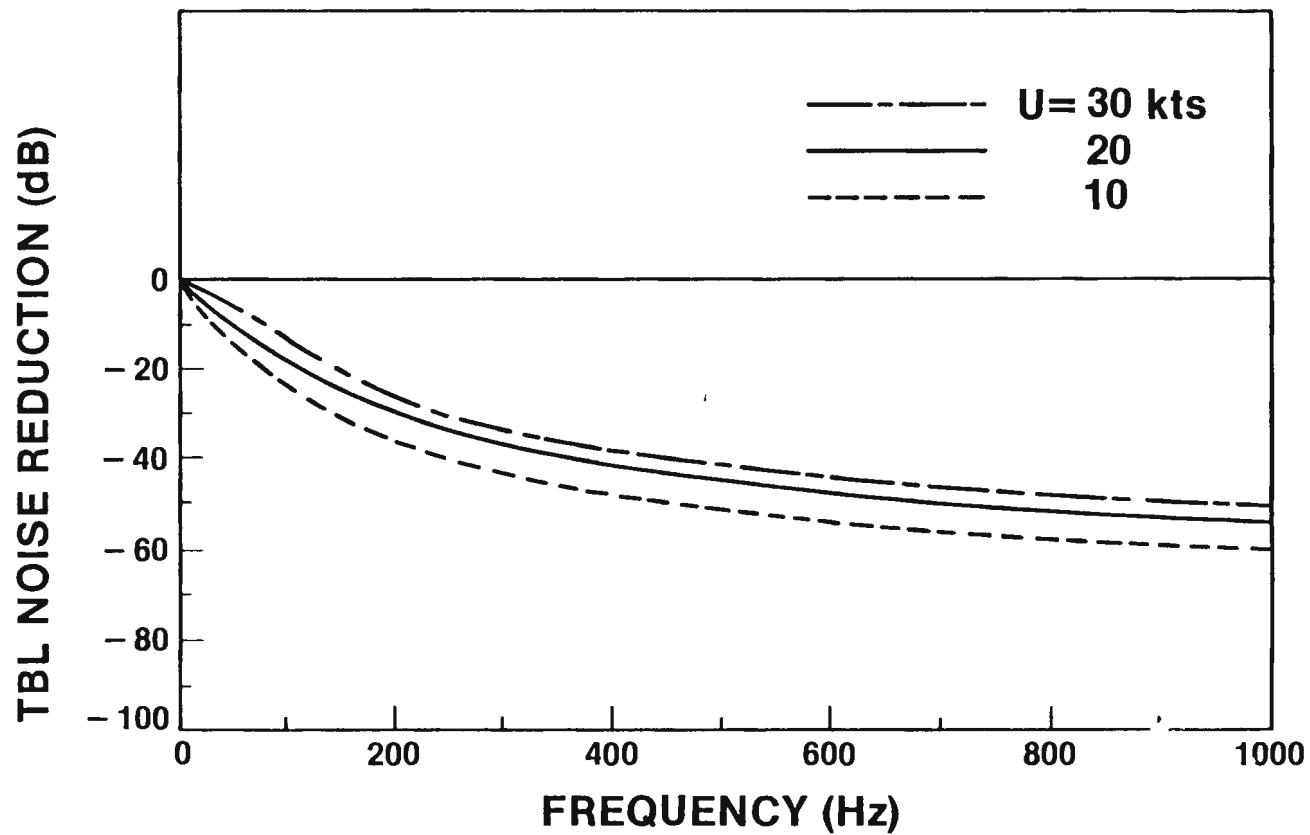


L4873eP

FIGURE 22



## EFFECT OF FREE STREAM VELOCITY (U)

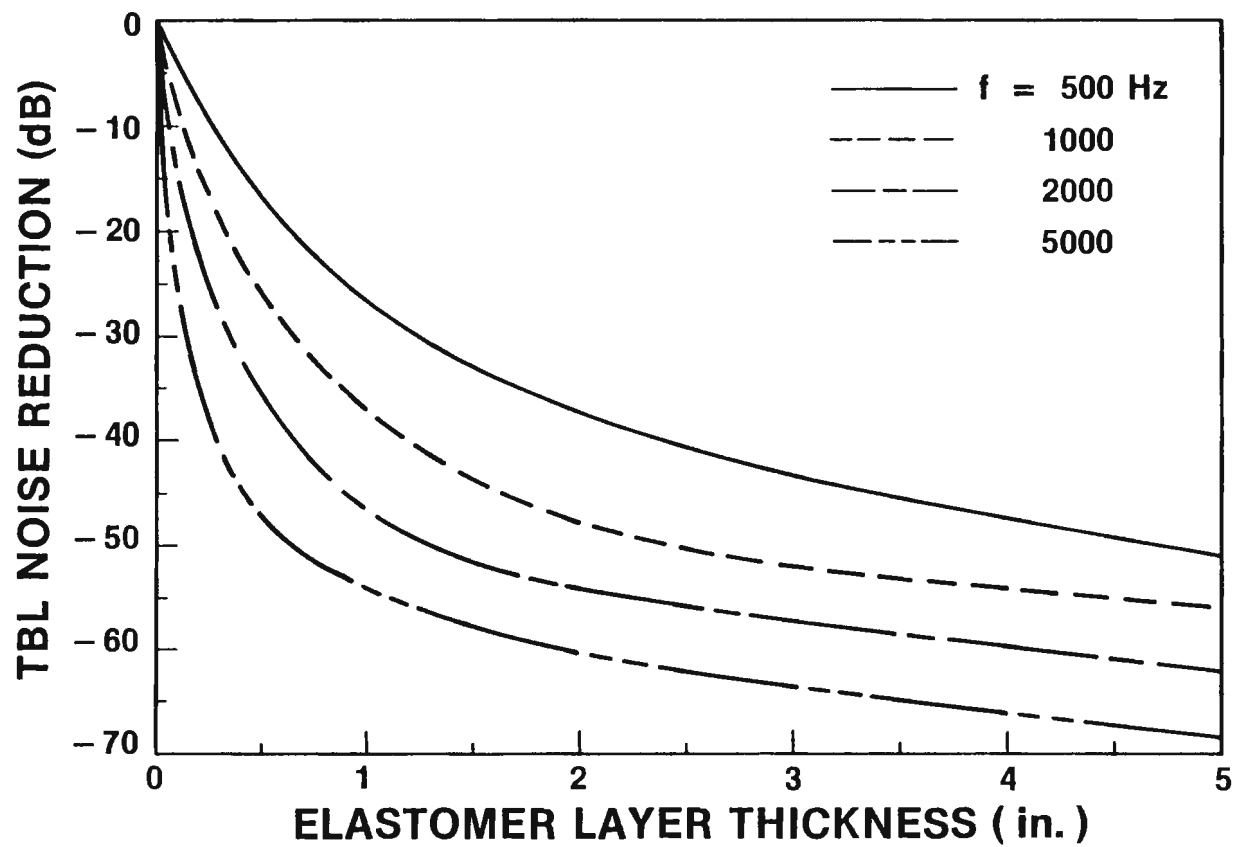


L4873cP

FIGURE 23



## EFFECT OF LAYER THICKNESS (h) (POINT HYDROPHONE)

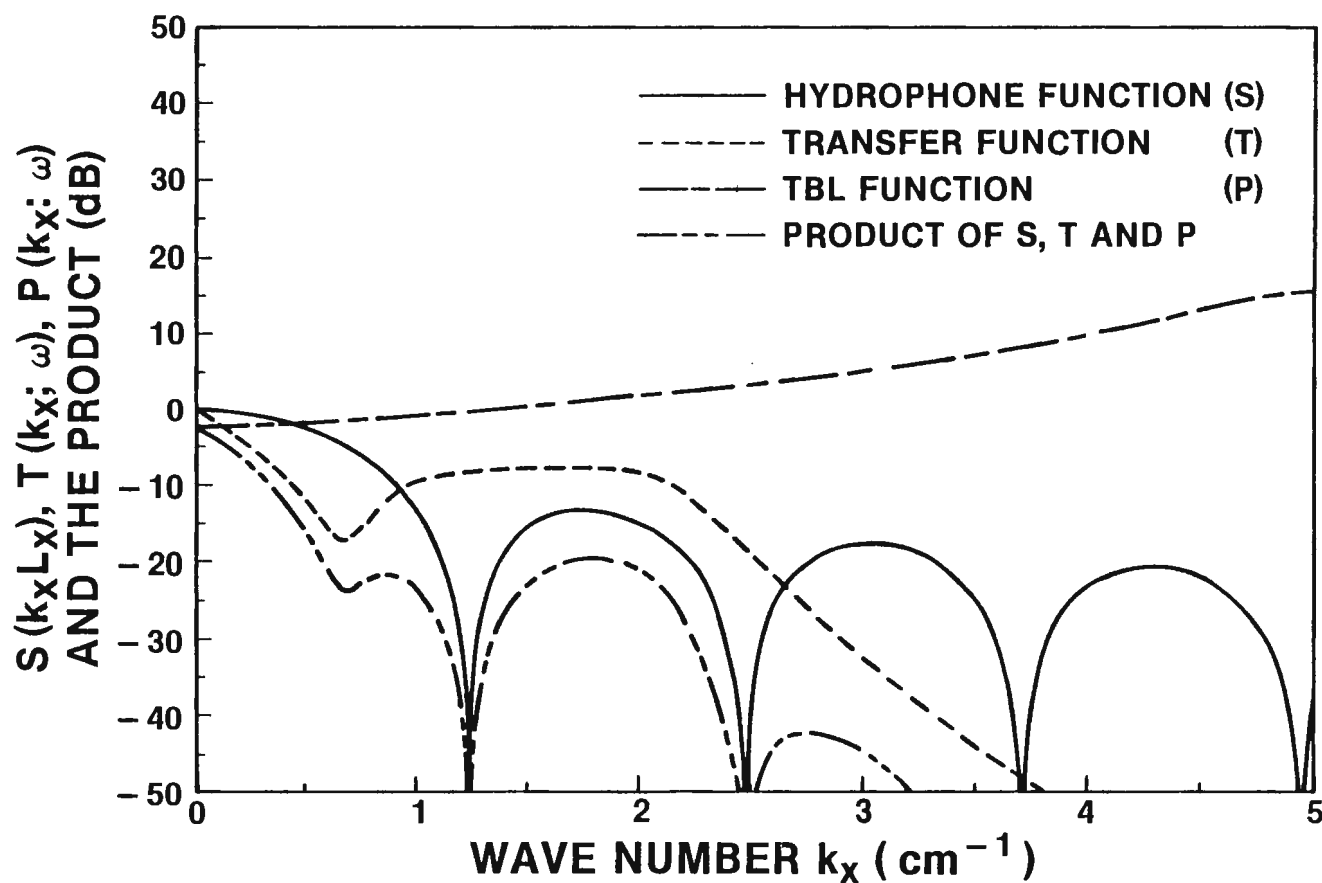


L50342oA

FIGURE 24



## RELEVANT FUNCTIONS (500 Hz)



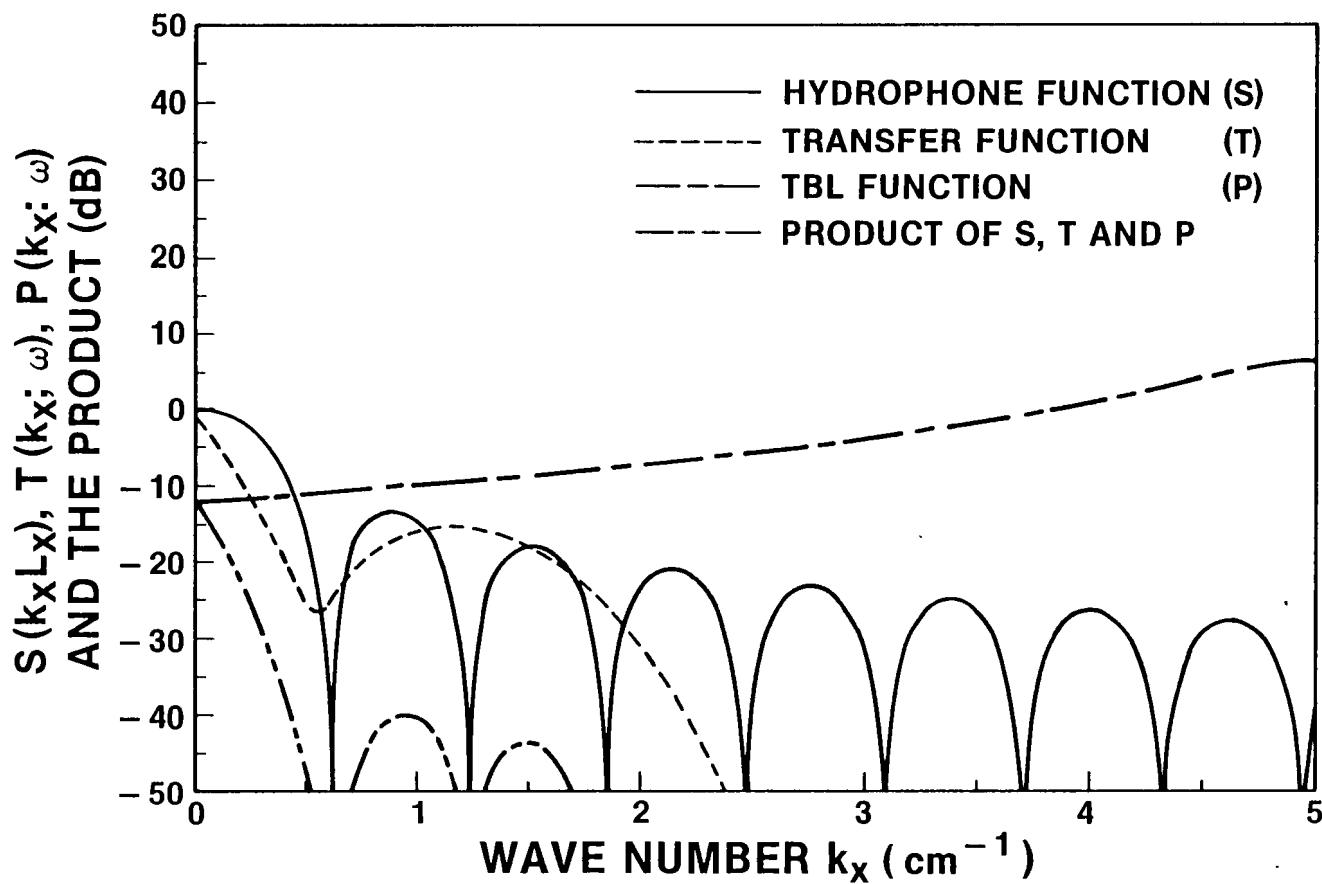
L50342gA

FIGURE 25

TM NO. 851103



## RELEVANT FUNCTIONS (1000 Hz)

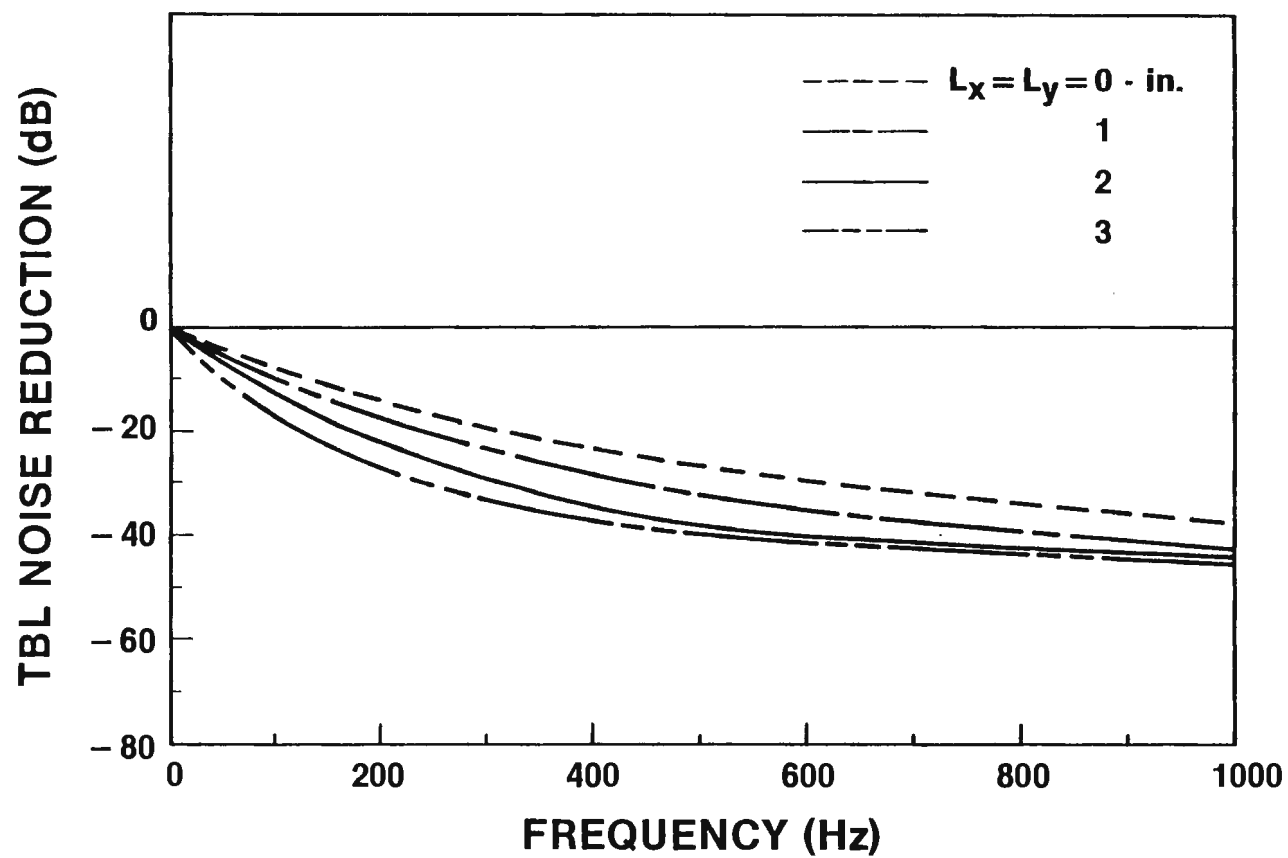


L50342hA

FIGURE 26



## EFFECT OF HYDROPHONE SIZE ( $L_x = L_y$ )

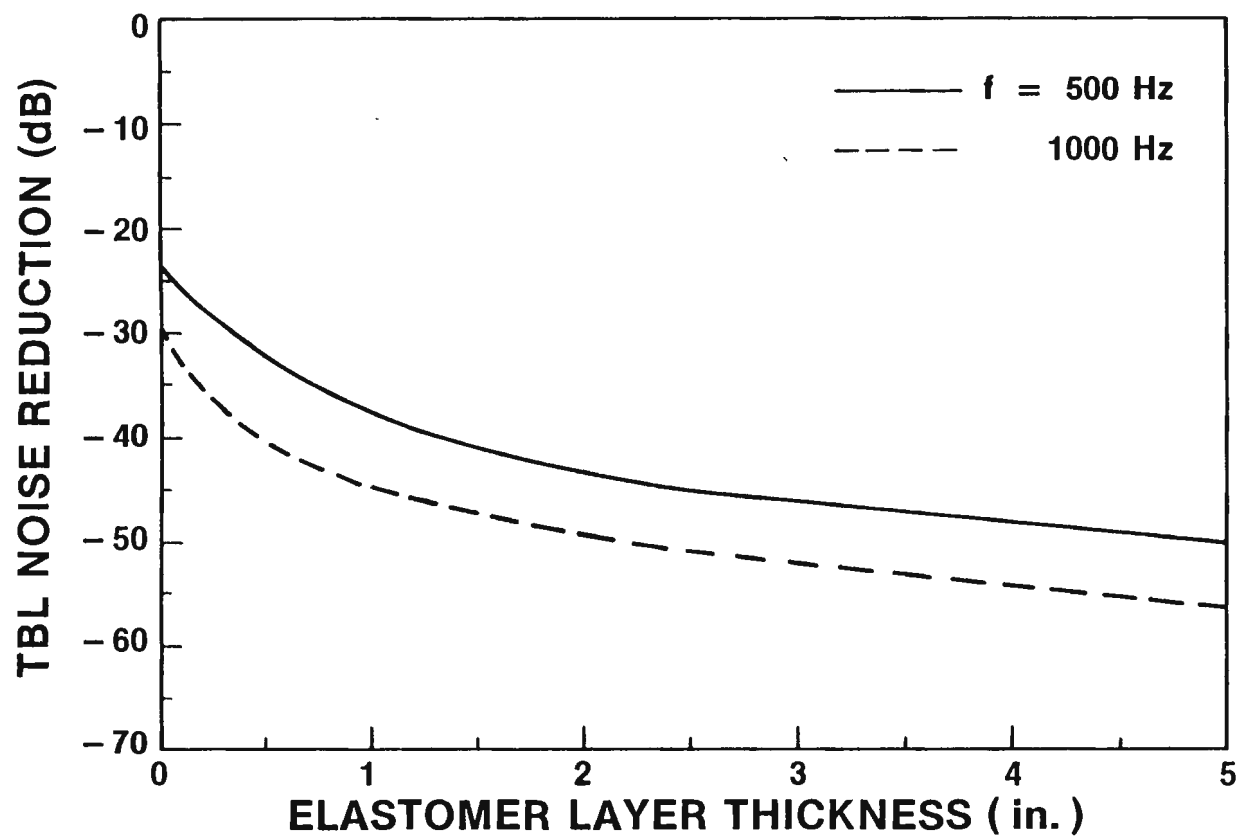


L50342qA

FIGURE 27



## EFFECT OF LAYER THICKNESS (h) (2-in. SQUARE HYDROPHONE)

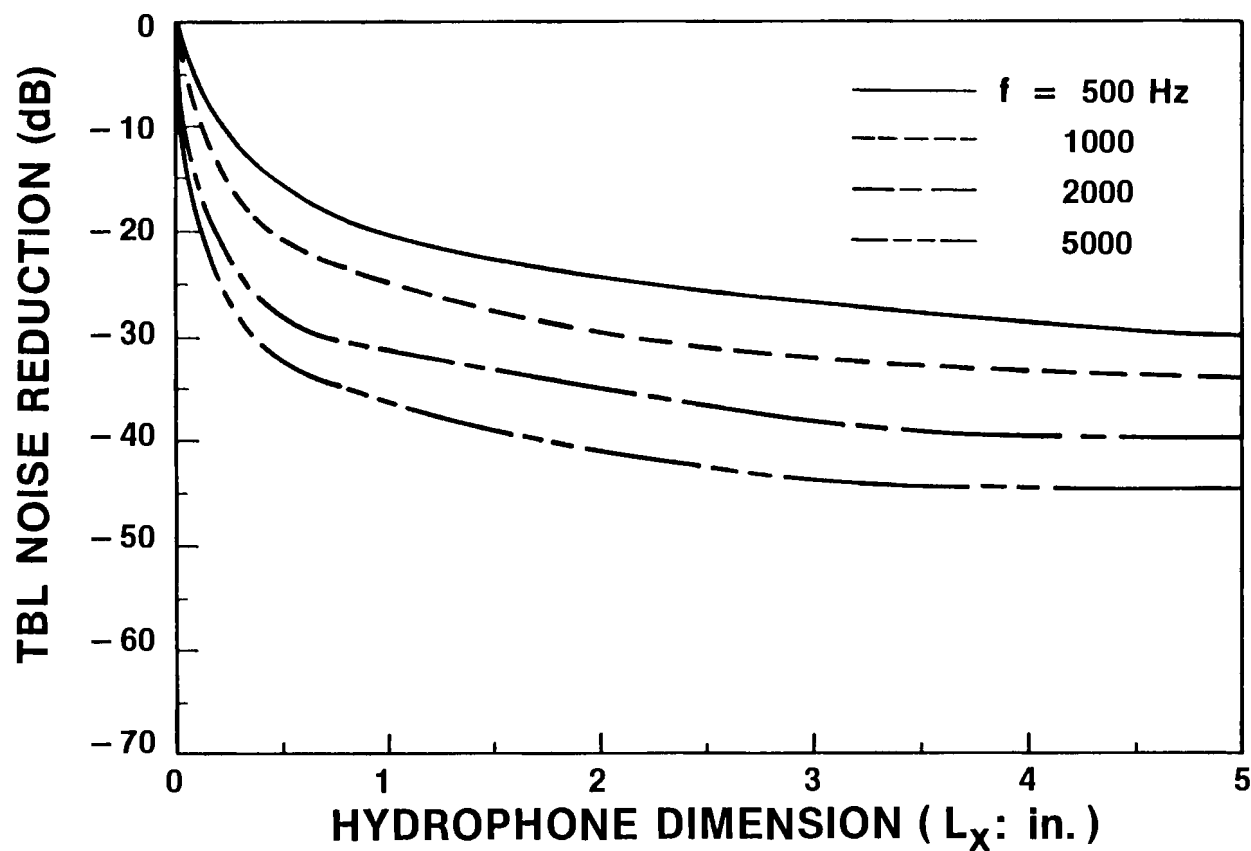


L50342mA

FIGURE 28



## EFFECT OF $L_x$ FOR $L_y = 0.5$ -in. (FLUSH MOUNTED HYDROPHONE)



L50342nA

FIGURE 29

TM NO. 851103



## **CONCLUSIONS (POINT HYDROPHONE)**

### **TBL NOISE DECREASES:**

#### **WHEN DECREASING**

- **STAND-OFF DISTANCE ( $d$ )**
- **FREE STREAM VELOCITY ( $U$ )**
- **SHEAR WAVE SPEED ( $c_{to}$ ) FOR HIGH FREQUENCY**

#### **WHEN INCREASING**

- **LOSS FACTOR ( $\zeta_s$ )**
- **ELASTOMER LAYER THICKNESS ( $h$ )**
- **SHEAR WAVE SPEED ( $c_{to}$ ) FOR LOW FREQUENCY**



## **CONCLUSIONS (FINITE HYDROPHONE)**

### **TBL NOISE DECREASES:**

#### **WHEN INCREASING**

- **HYDROPHONE SIZE ( SQUARE HYDROPHONE )**
- **RATIO  $L_x / L_y$  ( FOR A FIXED  $L_y$  )**

**ALL CONCLUSIONS DRAWN FOR THE POINT HYDROPHONE  
ARE ALSO VALID FOR FINITE HYDROPHONES.**

L50342fA

FIGURE 31



DEPARTMENT OF THE NAVY  
NAVAL UNDERWATER SYSTEMS CENTER

NEWPORT LABORATORY  
NEWPORT, RI 02841

NEW LONDON LABORATORY  
NEW LONDON, CT 06320

IN REPLY REFER TO:

5600

Ser 53233L/271

AUG 26 1985

From: Dr. S.H. Ko, Code 3233, Naval Underwater Systems Center, New London  
Laboratory, New London, CT 06320

To: Distribution

Subj: FORWARDING OF NUSC TECHNICAL MEMORANDUM NO. 851103 OF 21 JUNE 1985

Encl: (1) NUSC Technical Memorandum No. 851103, "Calculations of Turbulent  
Boundary Layer (TBL) Pressure Fluctuations transmitted into a  
Viscoelastic Layer", by Sung H. Ko and Howard H. Schloemer

1. Enclosure (1) is herewith forwarded for your information and retention.
2. This technical memorandum presents the text and vugraphs of an invited paper presented at the 109th Meeting of the Acoustical Society of America held in Austin, Texas on 8-12 April 1985.
3. Questions and/or comments regarding the subject memorandum should be addressed to Dr. Sung H. Ko, Code 3233; (203) 440-4786 or Dr. Howard H. Schloemer, Code 3233; (203) 440-4215, Naval Underwater Systems Center, New London Laboratory, New London, Connecticut 06320.

*Sung-Hwan Ko*  
DR. SUNG HWAN KO  
PHYSICIST

Distribution (w/encl.):

ONR (J. Webster, Code 280)  
DARPA (A. Ellinthorpe)  
DTNSRDC Bethesda (Dr. M. Sevik, Code 19)  
    (Dr. W. Blake, Code 1905.1)  
    (Dr. D. Feit, Code 1905.1)  
    (Dr. F. Archibald, Code 194)  
    (F. Geib, Code 1942)  
    (Dr. Y. Hwang, Code 1942)

Subj: FORWARDING OF NUSC TECHNICAL MEMORANDUM NO. 851103 OF 21 JUNE 1985.

Internal Distribution List:

Code 0302A	(Dr. R. Elswick)
Code 10	(Dr. W. Von Winkle)
Code 101	(Dr. E. Uram)
Code 32	(Dr. F. Kingsbury)
Code 3212	(Dr. D. Hurdis)
	(M. Ahmed)
	(M. Francoeur)
Code 323	(G. F. Carey)
	(Dr. W. Strawderman)
	(Dr. R. Kennedy)
Code 3232	(G. Connolly)
	(Dr. H. Bakewell)
	(Dr. R. Streit)
Code 3233	(Dr. H. Schloemer)
	(R. Christman)
	(B. Cray)
	(N. Dubois)
	(R. Dumont)
	(J. Gagne)
	(R. Gay)
	(J. Guigli)
	(M. Hill)
	(H. Jones)
	(S. Kavarnos)
	(Dr. S. Ko)
	(D. Legerski)
	(W. Maciejewski)
	(R. Maple)
	(V. Marolda)
	(D. McDowell)
	(S. Pappas)
	(E. Payne)
	(E. Recine)
Code 3233s	(w/o encl.)
Code 3234	(B. McTaggart)
	(C. LeBlanc)
	(J. Lindberg)
	(T. Meyers)
	(H. Miller)
	(D. Porter)
	(J. Powers)

Subj: FORWARDING OF NUSC TECHNICAL MEMORANDUM NO. 851103 OF 21 JUNE 1985

Internal Distribution List (Continued)

Code 3292	(Dr. C. Sherman)
	(B. Buehler)
Code 33	(L. Freeman)
Code 33A	(D. Power)
Code 33A4	(D.M. Ashworth)
Code 332	(Dr. R. Radlinski)
Code 3321	(Dr. R. Moffett)
	(R. Vogelsong)
Code 3322	(S. Rupinski)
	(Dr. E. Kuo)
Code 3323	(H. Phelps)
	(D. Bostian)
	(S. Traggis)
	(D. Walters)
Code 3635	(Dr. A Harari)
	(Dr. B. Sandman)
Code 4131	(P. Danforth)
Code 4492	(Dr. A. Kalinowski)
Code 0213	(New London Library) (5)
Code 02133	(Newport Library, Distribution Center) (5)

Writer: S. Ko, 3233, X4786  
Typist: V. Stanton, 20 Aug 85, X4180